

See discussions, stats, and author profiles for this publication at: <https://www.researchgate.net/publication/44605866>

Effects of Oxyanions, Natural Organic Matter, and Bacterial Cell Numbers on the Bioreduction of Lepidocrocite (γ -FeOOH) and the Formation of Secondary Mineralization Products

ARTICLE *in* ENVIRONMENTAL SCIENCE AND TECHNOLOGY · JUNE 2010

Impact Factor: 5.33 · DOI: 10.1021/es100294w · Source: PubMed

CITATIONS

54

READS

57

5 AUTHORS, INCLUDING:



Edward J. O'Loughlin

Argonne National Laboratory

64 PUBLICATIONS 2,475 CITATIONS

[SEE PROFILE](#)



Michelle Scherer

University of Iowa

83 PUBLICATIONS 4,112 CITATIONS

[SEE PROFILE](#)



Maxim Boyanov

Bulgarian Academy of Sciences

83 PUBLICATIONS 1,464 CITATIONS

[SEE PROFILE](#)

Effects of Oxyanions, Natural Organic Matter, and Bacterial Cell Numbers on the Bioreduction of Lepidocrocite (γ -FeOOH) and the Formation of Secondary Mineralization Products

EDWARD J. O'LOUGH LIN,^{*†}CHRISTOPHER A. GORSKI,[‡]MICHELLE M. SCHERER,[‡]MAXIM I. BOYANOV,[†] ANDKENNETH M. KEMNER[†]

Biosciences Division, Argonne National Laboratory, Argonne, Illinois 60439-4843, and Department of Civil and Environmental Engineering, University of Iowa, Iowa City, Iowa 52242-1527

Received January 27, 2010. Revised manuscript received May 5, 2010. Accepted May 7, 2010.

Microbial reduction of Fe(III) oxides results in the production of Fe(II) and may lead to the subsequent formation of Fe(II)-bearing secondary mineralization products including magnetite, siderite, vivianite, chukanovite (ferrous hydroxy carbonate (FHC)), and green rust; however, the factors controlling the formation of specific Fe(II) phases are often not well-defined. This study examined effects of (i) a range of inorganic oxyanions (arsenate, borate, molybdate, phosphate, silicate, and tungstate), (ii) natural organic matter (citrate, oxalate, microbial extracellular polymeric substances [EPS], and humic substances), and (iii) the type and number of dissimilatory iron-reducing bacteria on the bioreduction of lepidocrocite and formation of Fe(II)-bearing secondary mineralization products. The bioreduction kinetics clustered into two distinct Fe(II) production profiles. "Fast" Fe(II) production kinetics [19–24 mM Fe(II) d⁻¹] were accompanied by formation of magnetite and FHC in the unamended control and in systems amended with borate, oxalate, gellan EPS, or Pony Lake fulvic acid or having "low" cell numbers. Systems amended with arsenate, citrate, molybdate, phosphate, silicate, tungstate, EPS from *Shewanella putrefaciens* CN32, or humic substances derived from terrestrial plant material or with "high" cell numbers exhibited comparatively slow Fe(II) production kinetics [1.8–4.0 mM Fe(II) d⁻¹] and the formation of green rust. The results are consistent with a conceptual model whereby competitive sorption of more strongly bound anions blocks access of bacterial cells and reduced electron-shuttling compounds to sites on the iron oxide surface, thereby limiting the rate of bioreduction.

Introduction

The biogeochemical cycling of Fe in aquatic and terrestrial environments is complex, involving a suite of highly inter-

dependent biotic and abiotic processes. For example, microbial reduction of Fe(III) oxides results in the production of Fe(II) and may lead to formation of Fe(II)-bearing secondary mineralization products including magnetite, siderite, vivianite, chukanovite (ferrous hydroxy carbonate (FHC)), and green rust. Green rusts—mixed Fe(II)/Fe(III) layered double hydroxides—have been reported as products of the bioreduction of Fe(III) oxides in laboratory-based studies (1–13), as well as in Fe(III)/Fe(II) transition zones in natural systems (14–18).

The factors controlling formation of specific Fe(II) phases as a consequence of microbial Fe(III) reduction are complex and not fully understood; however, the rate and magnitude of Fe(II) production and its reaction with residual Fe(III) phases and other ligands (e.g., phosphate, carbonate) are often cited as primary factors (2, 19–23). In laboratory experiments with single Fe(III) oxide phases, the formation of green rust as a secondary mineralization product is typically linked to phosphate concentration or the number of dissimilatory iron-reducing bacteria (IRB) present (1, 2, 5, 11, 13). In natural systems, the factors contributing to green rust formation have yet to be identified. Soils and sediments contain a range of organic and inorganic ligands (e.g., inorganic oxyanions such as phosphate and silicate, as well as natural organic matter [NOM] ranging from low-molecular-mass aliphatic acids to high-molecular-mass biopolymers and humic substances) that are known to affect Fe(II)/Fe(III) redox transformations and accompanying changes in Fe speciation (24); however, their potential role in the formation of green rusts in these environments is uncertain. For example, a green rust phase was identified by X-ray absorption spectroscopy analysis of Fe-rich lacustrine sediments containing high As levels (18), although what role, if any, As played in formation of green rust in these sediments remains unclear.

To better understand the factors contributing to the formation of green rust as a secondary mineralization product of the bioreduction of Fe(III) oxides, we examined the effects of (i) the oxyanions arsenate, borate, molybdate, phosphate, silicate, and tungstate; (ii) NOM including aliphatic acids (citrate and oxalate), humic substances (Elliott soil humic acid [ESHA], leonardite humic acid [LHA], Pony Lake fulvic acid [PLFA], Suwannee River fulvic acid [SRFA], and Suwannee River humic acid [SRHA]), and microbially produced extracellular polymeric substances (EPS); and (iii) the type and number of bacterial cells on the bioreduction of lepidocrocite (γ -FeOOH) and the accompanying formation of Fe(II)-bearing secondary mineralization products.

Experimental Section

Details on the sources of chemicals, synthesis and characterization of lepidocrocite, and isolation of EPS produced by *Shewanella putrefaciens* CN32 (hereafter designated CN32 EPS) are in the Supporting Information. The experimental systems consisted of sterile 160 mL serum vials containing 100 mL of sterile defined mineral medium (DMM) (6) with Fe(III) as lepidocrocite (80 mM), formate (75 mM), and anthraquinone-2,6-disulfonate (AQDS) (100 μ M); the levels of lepidocrocite and formate were chosen to provide sufficient material for frequent sampling over the course of the experiments and to ensure that electron donor limiting conditions did not develop. DMM was prepared by combining all components except formate, AQDS, and oxyanions/NOM. The pH was adjusted to 7.5, and the medium was autoclaved. After the medium cooled to ambient temperature,

* Corresponding author phone: 630-252-9902; fax: 630-252-9793; e-mail: oloughlin@anl.gov.

[†] Argonne National Laboratory.

[‡] University of Iowa.

TABLE 1. Fe(II) Production Rates^a and Identification of Secondary Mineralization Products Based on XRD, ⁵⁷Fe Mössbauer Spectroscopy, and SEM Imaging

system	Fe(II) production rate		identification of secondary mineralization products ^b		
	mM Fe(II) d ⁻¹	kinetic profile ^c	XRD	Mössbauer	SEM ^d
no amendment	21.66 ± 0.87	fast	Mag ^e , FHC ^f (trace)	Mag, FHC	Mag, FHC (minor)
Oxyanions					
arsenate (500 μM)	2.19 ± 0.096	slow	GR ^g	GR	GR
borate (500 μM)	21.09 ± 3.36	fast	Mag, FHC (trace)	Mag, FHC	Mag, FHC (minor)
borate (5 mM)	21.39 ± 3.13	fast	Mag, FHC (trace)	ND ^h	Mag, FHC (minor)
molybdate (500 μM)	2.44 ± 0.102	slow	GR	GR	GR
phosphate (500 μM)	2.85 ± 0.154	slow	GR	GR	GR
silicate (500 μM)	2.63 ± 0.122	slow	GR	GR	GR
tungstate (500 μM)	2.56 ± 0.132	slow	GR	GR	GR
Natural Organic Matter					
citrate (500 μM)	2.41 ± 0.180	slow	GR	GR	GR
oxalate (500 μM)	21.55 ± 1.37	fast	Mag, FHC (trace)	Mag, FHC	Mag, FHC (minor)
oxalate (5 mM)	20.74 ± 1.33	fast	Mag, FHC (trace)	ND	Mag, FHC (minor)
Elliott soil humic acid (20 mg L ⁻¹)	2.21 ± 0.117	slow	GR	ND	GR
leonardite humic acid (20 mg L ⁻¹)	2.42 ± 0.144	slow	GR	ND	GR
Pony Lake fulvic acid (20 mg L ⁻¹)	25.14 ± 3.93	fast	Mag, FHC (trace)	ND	Mag, FHC (minor)
Suwannee River fulvic acid (20 mg L ⁻¹)	1.81 ± 0.043	slow	GR	ND	GR
Suwannee River humic acid (20 mg L ⁻¹)	2.61 ± 0.237	slow	GR	GR	GR
EPS from <i>S. putrefaciens</i> CN32 (100 mg L ⁻¹)	2.54 ± 0.265	slow	GR	ND	GR
gellan (100 mg L ⁻¹)	26.23 ± 1.14	fast	Mag, FHC (trace)	ND	Mag, FHC (minor)
Biomass					
<i>S. putrefaciens</i> ATCC 8071 (5 × 10 ⁹ cells mL ⁻¹)	19.84 ± 2.56	fast	Mag, FHC (trace)	ND	ND
<i>S. putrefaciens</i> ATCC 8071 (1 × 10 ¹⁰ cells mL ⁻¹)	4.00 ± 0.255	fast	GR	ND	ND
<i>S. putrefaciens</i> CN32 (5 × 10 ⁹ cells mL ⁻¹)	21.66 ± 0.87	fast	Mag, FHC (trace)	Mag, FHC	Mag, FHC (minor)
<i>S. putrefaciens</i> CN32 (1 × 10 ¹⁰ cells mL ⁻¹)	24.26 ± 6.35	fast	Mag, FHC (trace)	ND	ND
<i>S. putrefaciens</i> CN32 (2 × 10 ¹⁰ cells mL ⁻¹)	3.66 ± 0.400	slow	GR	ND	ND

^a Fe(II) production rates calculated by linear regression using least-squares regression of the data during the period of maximum sustained Fe(II) production. ^b Additional information on the results of XRD (Figures S3–S6), Mössbauer spectroscopy (Table S3) and SEM imaging (Figures S7–S12) is in Supporting Information. ^c Fe(II) production profiles designated as “fast” or “slow” as described in the Results section. ^d Identification based on particle morphology. ^e Magnetite (Mag). ^f Ferrous hydroxy carbonate (FHC). ^g Green rust (GR). ^h Not determined (ND).

formate and AQDS were added from filter-sterilized stock solutions. The medium was then portioned into sterile serum bottles, and NOM or oxyanions were added to achieve the concentrations indicated in Table 1. The bottles were sealed with Teflon-lined rubber septa and aluminum crimp caps and sparged with sterile Ar to remove molecular oxygen. All systems were prepared in duplicate.

The inoculum was prepared from late-log-phase cultures of *S. putrefaciens* strain CN32 (ATCC BAA-543) or *S. putrefaciens* strain 8071 (ATCC 8071) as described by O’Loughlin et al. (7). Experiments were initiated by spiking each vial with the volume of inoculum needed to achieve the desired cell density (5 × 10⁹ cells mL⁻¹ of *S. putrefaciens* CN32 unless otherwise indicated). The effect of metabolically inactive cells on the abiotic reduction of lepidocrocite was determined with H₂ as the reductant in the presence of Pd catalyst as described by O’Loughlin (6), with the addition of pasteurized (70 °C for 1 h) *S. putrefaciens* CN32 cells. The suspensions were placed on a roller drum and incubated at 30 °C in the dark. Samples of the suspensions—for monitoring pH and Fe(II), as well as for identification of secondary mineralization products by X-ray diffraction (XRD), scanning electron microscopy (SEM), and ⁵⁷Fe Mössbauer spectroscopy (see Supporting Information for details)—were collected with sterile syringes. Unless otherwise indicated, sample collection and processing were conducted in a glovebox containing an anoxic atmosphere (95% N₂ with 5% H₂).

Results

Bioreduction of Lepidocrocite. Lepidocrocite was readily bioreduced by *S. putrefaciens* CN32 in unamended DMM. After inoculation, Fe(II) production commenced without a significant lag, reaching a concentration of 25 mM within

24 h and remaining at 25–30 mM for the duration of the experiment (Figure 1A). XRD analysis of the solids remaining 50 d after inoculation indicated complete removal of lepidocrocite, with formation of magnetite and traces of FHC (Figure 2). Analysis of the solids by Mössbauer spectroscopy (Figure 3) also indicated complete removal of lepidocrocite and the formation of magnetite (86% of total Fe) and FHC (14% of total Fe); the corresponding Mössbauer hyperfine parameters are listed in Table S3 (Supporting Information). SEM imaging of the solids (Figures 4A and 4B) showed the presence of rounded, cubic crystallites (~50 nm), consistent with fine-grained magnetite commonly observed as a secondary mineralization product of Fe(III) oxide bioreduction (2, 5, 25–28), as well as platy, micrometer-sized crystallites with a morphology consistent with FHC formed by bioreduction of a ferrihydrite-akaganéite mixture (26).

Phosphate binds strongly to Fe(III) oxides through formation of inner-sphere complexes (24) known to affect the stability and subsequent transformations of Fe(III) oxides (including biotic and abiotic reduction) (13, 29, 30). The addition of phosphate (500 μM) significantly affected lepidocrocite bioreduction (Figure 1A). Initially, Fe(II) production was suppressed; only 3 mM of Fe(II) was produced within the first 24 h (compared to 25 mM of Fe(II) in the absence of P), and significant additional Fe(II) production was not observed until day 5. The concentration of Fe(II) increased through day 32, then remained at 56–61 mM. The bioreduction of lepidocrocite in the presence of 500 μM phosphate resulted in the formation of green rust, as indicated by XRD and Mössbauer analysis of the solids (Figures 2 and 3); neither magnetite nor FHC was observed. The solids consisted primarily of platy hexagonal particles nominally 0.2 μm thick and up to 3 μm across (Figure 4C), having an overall

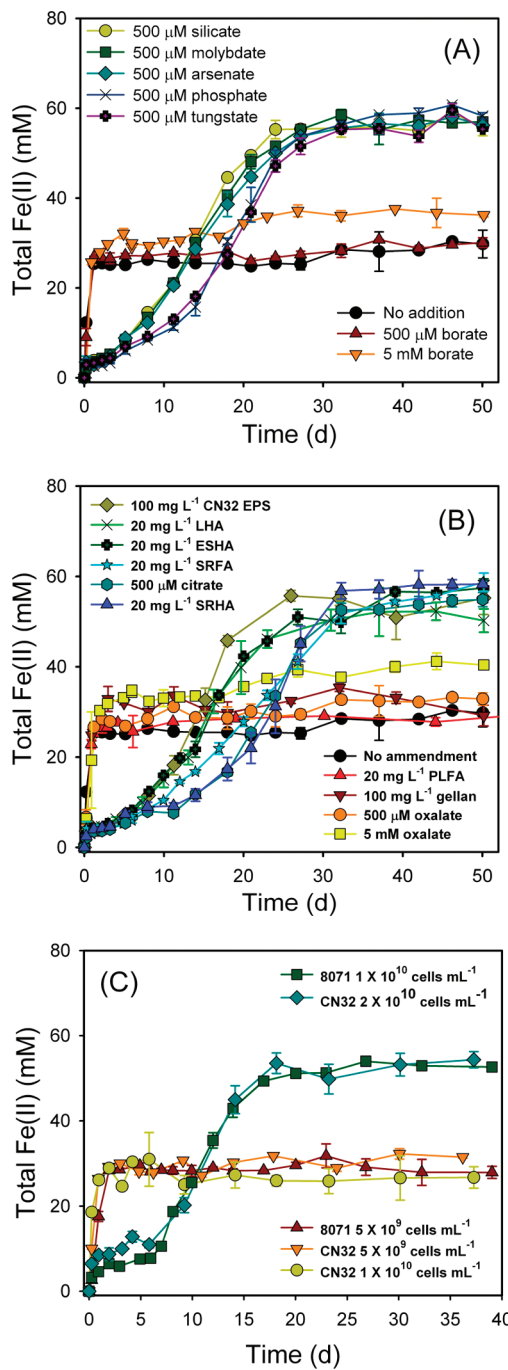


FIGURE 1. Production of Fe(II) during the bioreduction of 80 mM lepidocrocite by *S. putrefaciens* CN32 in the presence and absence of oxyanions (A) and NOM (B) and in the presence of various cell numbers of *S. putrefaciens* strains CN32 and ATCC 8071 (C). Lines are a visual aid only. Error bars indicate the average deviation.

morphology consistent with biogenic green rust (2, 5, 7, 8, 10). The addition of 500 μM of arsenate, molybdate, silicate, or tungstate had similar effects on the kinetics and overall extent of Fe(II) production, and (as with phosphate) resulted in green rust formation (Table 1). In contrast, with either 500 μM or 5 mM borate added, Fe(II) production kinetics were similar to those for the unamended system—but with slightly higher Fe(II) production with 5 mM borate (Figure 1A)—with formation of magnetite and FHC (Table 1).

Lepidocrocite bioreduction was also examined in systems containing organic ligands representing different components of NOM, including aliphatic acids, humic substances,

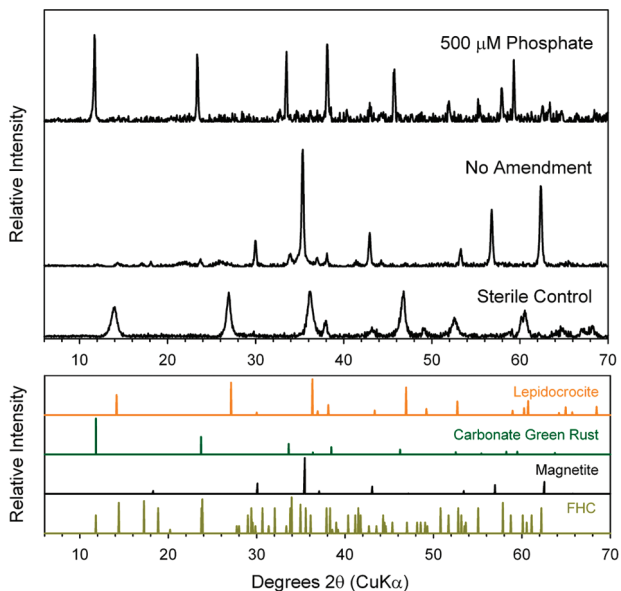


FIGURE 2. XRD patterns of solids in the sterile control and biominerization products resulting from the reduction of lepidocrocite in the unamended and 500 μM phosphate-amended experimental systems, compared with reference patterns of lepidocrocite, carbonate green rust, magnetite, and FHC.

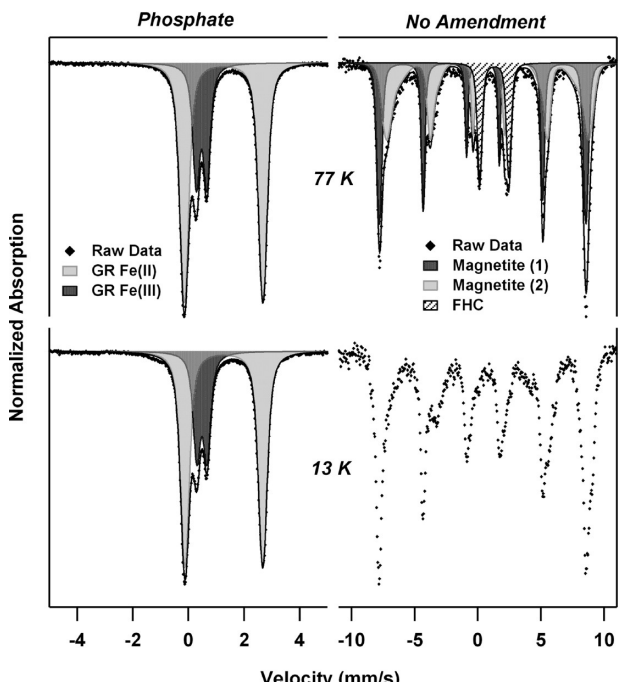


FIGURE 3. ⁵⁷Fe Mössbauer spectra of the biominerization products resulting from the reduction of lepidocrocite in the unamended (right) and 500 μM phosphate-amended (left) experimental systems. The raw data (◆) are presented with the least-squares fit overlaid (shaded areas) and total fit (—). The 13 K spectrum for the unamended system could not be fitted because of magnetic ordering of the FHC doublet to an octet. The presented spectra are representative of the other amended systems.

and microbially produced EPS. As with the inorganic oxyanions, the kinetics of Fe(II) production clustered into two distinct profiles (Figure 1B). Fe(II) production in the systems containing oxalate (either 500 μM or 5 mM), gellan, or PLFA tracked with the unamended control, exhibiting a rapid increase in Fe(II) concentration that quickly leveled off at

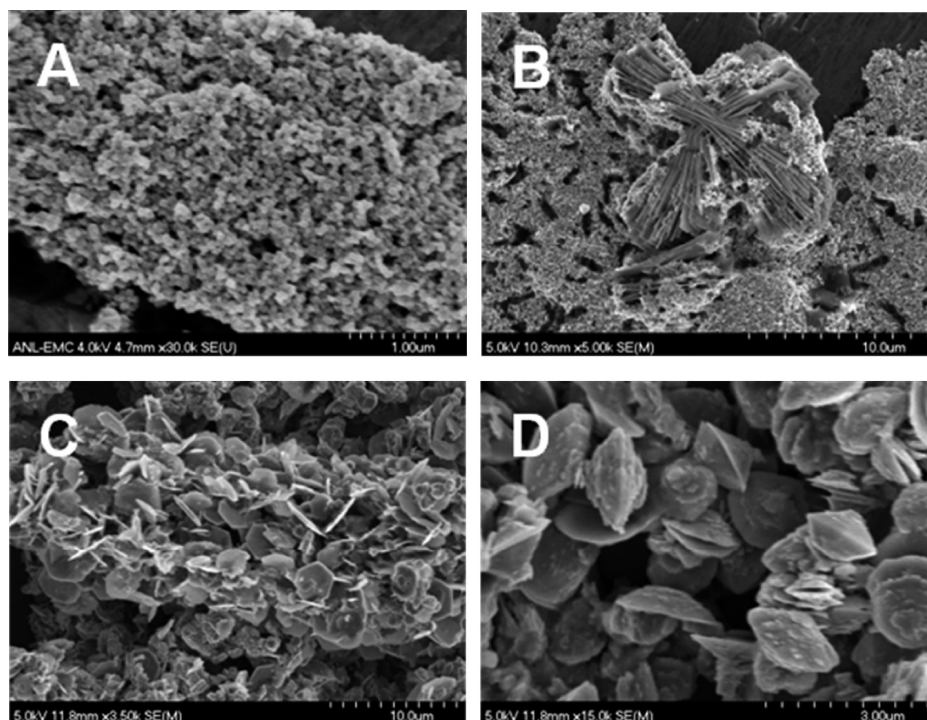


FIGURE 4. SEM images of magnetite (**A**) and magnetite/FHC (**B**) formed in the unamended system and of green rust formed in the systems containing 500 μM phosphate (**C**) and 20 mg L^{-1} ESHA (**D**).

25–30 mM (~40 mM for 5 mM oxalate; which may have been due, in part, to oxalate-enhanced lepidocrocite dissolution). Magnetite and FHC were the only secondary mineralization products observed in these systems (Table 1). The addition of citrate, ESHA, LHA, SRFA, SRHA, or CN32 EPS resulted in Fe(II) production profiles similar to those for the arsenate, molybdate, phosphate, silicate, and tungstate systems. An initial pulse of 3–4.6 mM Fe(II) within the first 24 h was followed by a 3–5 d pause, then increasing Fe(II) concentrations through days 6–31; after this, Fe(II) concentrations remained relatively constant at 52–58 mM. Green rust was the only identified secondary mineralization product in each of these systems (Table 1). In contrast to the platy habit typically reported for green rust, and evident in the green rusts formed in the arsenate, molybdate, phosphate, silicate, tungstate, citrate, and CN32 EPS-amended systems (Figure 4C and Figures S8–10, and S12, Supporting Information), the green rusts in the LHA-, SHA-, SRFA-, and SRHA-amended systems exhibited pyramidal and prismatic habits (Figure 4D and Figure S11, Supporting Information), similar to that of several related, layered double hydroxides of the hydrotalcite group (31).

Altering the number and type of bacterial cells resulted in the same two types of Fe(II) production profiles as observed with the inorganic oxyanions and NOM. Initial cell loadings of 5×10^9 cells mL^{-1} for *S. putrefaciens* strains 8071 or CN32 resulted in rapid Fe(II) production (Figure 1C) and formation of magnetite and FHC (Table 1). Cell loadings of 1×10^{10} cells mL^{-1} of *S. putrefaciens* CN32 also exhibited rapid Fe(II) production and magnetite/FHC formation, while the same loading of *S. putrefaciens* 8071 resulted in slower Fe(II) production, higher final Fe(II) concentration, and the formation of green rust. Increasing *S. putrefaciens* CN32 to 2×10^{10} cells mL^{-1} resulted in “slow” Fe(II) production kinetics and green rust formation. The effects of *S. putrefaciens* CN32 cell density were the same regardless of the metabolic state of the cells. We examined the effects of metabolically inactive (dead) cells on lepidocrocite reduction of by H_2/Pd catalyst in the presence of AQDS. As in the experiments with live cells, the addition of 5×10^9 or 1×10^{10} cells mL^{-1} of

pasteurized *S. putrefaciens* CN32 resulted in formation of magnetite, and green rust formed with 2×10^{10} cells mL^{-1} (Figure S6, Supporting Information). These results demonstrate that the levels of biomass (whether metabolically active or dead) or cell products (such as EPS) can have a significant effect on Fe(III) oxide reduction and subsequent secondary mineralization product formation and that cell density effects may be species specific. Our results are generally consistent with a previous study by Zegeye et al. (11), which showed similar cell number effects on secondary mineralization product formation during lepidocrocite bioreduction by *S. putrefaciens* CIP 8040 (equivalent to ATCC 8071).

Lepidocrocite bioreduction was complete in all of the experimental systems to the extent that no lepidocrocite was detected at the end of the experiments. However, substantial Fe(III) remained after Fe(II) production ceased; ~37–75% of Fe(III) was reduced to Fe(II), of which >98% was present in the solids. The overall extent of Fe(III) reduction appears to be constrained by the incorporation of Fe(III) into specific secondary mineralization products. The lower overall extent of Fe(II) production [~30–41 mM Fe(II)] observed in the systems with “rapid” Fe(II) production profiles (Figure 1) is consistent with formation of magnetite as the major product, as magnetite nominally has an Fe(III):Fe(II) ratio of 2. Systems with “slow” Fe(II) production profiles had higher overall Fe(II) levels [~52–60 mM Fe(II)], consistent with the formation of green rust, which, although variable, has a nominal Fe(III):Fe(II) ratio of 0.5. Under the appropriate conditions or given sufficient time, the Fe(III) in magnetite and green rust can be bioreduced (9, 32); however, incorporation of Fe(III) into these phases effectively rendered it unavailable for use by *S. putrefaciens* as a terminal electron acceptor for anaerobic respiration in our experiments.

Discussion

Although this study was primarily a phenomenological investigation of the effects of various organic and inorganic ligands on lepidocrocite bioreduction and secondary mineralization product formation rather than an in-depth

mechanistic treatment, our results do offer new insight that provides a basis for discussion of possible controls on Fe(III) oxide bioreduction and product formation. In particular, the distinct clustering of the Fe(II) production kinetics into a “fast” profile leading to magnetite/FHC or a “slow” profile leading to green rust is suggestive of a common underlying mechanism. Many studies have identified green rust as a product of Fe(III) oxide bioreduction (1–13); however, few have explicitly identified the factor(s) leading to green rust formation at the expense of other products such as magnetite. The presence of phosphate (2), or more directly, the extent of phosphate sorption to Fe(III) oxides (1, 13), has been identified as the key factor in the formation of green rust (instead of magnetite) following the bioreduction of ferrihydrite by *S. putrefaciens* CN32; however, the mechanism by which phosphate leads to green rust formation is not clear (i.e., whether phosphate explicitly suppresses magnetite formation or promotes green rust formation). Zegeye et al. (11) proposed that the formation of green rust versus magnetite is controlled by the rate of Fe(III) oxide bioreduction, with faster rates promoting the formation of magnetite; which is consistent with magnetite formation in our experimental systems exhibiting “fast” Fe(II) production profiles versus green rust formation in systems with “slow” Fe(II) production profiles. However, it is still unclear whether the Fe(II) production rate really is the controlling factor or merely a consequence of other processes having more direct control on secondary mineralization product formation.

Given the relatively low solubility of Fe(III) oxides, lepidocrocite bioreduction in our experimental system is driven by transfer of electrons from components of the respiratory chain in *S. putrefaciens* CN32 to the oxide surface—both directly, via contact of the cell surface with the oxide, and indirectly by microbial reduction of AQDS to anthrahydroquinone-2,6-disulfonate (AH₂QDS) and subsequent reduction of the oxide by AH₂QDS. Indeed, *S. oneidensis* MR-1, a species closely related to *S. putrefaciens* CN32 (7), binds to hematite via inner-sphere complexation of phosphoryl groups to Fe centers on the oxide surface (33). Moreover, MtrC and Omca, outer membrane cytochromes that are key components in the transfer of electrons from the interior of the cell to external electron acceptors like Fe(III) oxides, bind to hematite (34) and, as shown for Omca, remain catalytically active (i.e., can transfer electrons from an electron donor like NADH to the oxide) (35). Both direct and indirect reduction processes require access to surface sites on the oxide; therefore, binding of competing ligands to Fe(III) oxides can potentially decrease the rate of Fe(II) production by limiting access of bacterial cells and AH₂QDS to surface sites on Fe(III) oxides where electron transfer occurs. For example, the competitive binding of phosphate limits the reduction of hematite by AH₂QDS (30).

An in-depth discussion of the multiple factors controlling the sorption of the various ligands examined in this study to Fe(III) oxides is beyond the scope of this paper; however, an overview of the topic indicates substantial variability in the extent and mechanisms of ligand binding to Fe(III) oxides (24). A comparison of the Fe(II) production rates and corresponding secondary mineralization product formation (Table 1) with the uptake of 500 μM of arsenate, borate, citrate, molybdate, oxalate, phosphate, silicate, and tungstate by lepidocrocite (Figure S13, Supporting Information) is consistent with the premise that the extent of anion sorption constrains Fe(III) oxide bioreduction (13). However, the uptake of 5 mM borate or oxalate was comparable to that of the other anions at 500 μM, and yet Fe(II) production kinetics and secondary mineralization product formation were nominally the same as for the unamended system. These results may be a consequence of relative differences in the strength of anion binding and/or binding to different sites

on lepidocrocite. An overview of the literature regarding the sorption of arsenate, borate, citrate, molybdate, oxalate, phosphate, silicate, and tungstate to Fe(III) oxides indicates that all typically form inner-sphere complexes (Table S2, Supporting Information); however, the relative strength of binding among these anions is highly variable. Although few studies have explicitly examined the competitive binding of the anions examined in this study to iron oxides, reported data indicate that borate and oxalate bind less strongly than arsenate, citrate, phosphate, and silicate (29, 36–38) and therefore might be more easily displaced by bacteria or AH₂QDS—consistent with the lack of inhibition of lepidocrocite bioreduction, even when levels of sorbed borate and oxalate were greater than levels of adsorbed arsenate, citrate, molybdate, phosphate, silicate, and tungstate.

Similar considerations may contribute to the differences in Fe(II) production kinetics and secondary mineralization product formation among the various NOM fractions. The general trend for the binding of NOM by iron oxides is for preferential sorption of aromatic over aliphatic, hydrophobic over hydrophilic, and larger over smaller molecules (24). Therefore, given the relative differences in aromaticity and molecular mass among the humic substances examined in this study (Table S1, Supporting Information), it is perhaps not surprising that the more aromatic and larger humics, derived primarily from the degradation of terrestrial plants and thus containing a significant fraction of lignin residues, exhibited the same kinetic profile and secondary mineralization product formation as the strongly adsorbing anions, while the less aromatic and lower-molecular-mass PLFA, derived from microbial biomass consisting primarily of polypeptides and polysaccharides, exhibited Fe(II) production kinetics and product formation similar to borate- and oxalate-amended systems. Likewise, the different effects observed with CN32 EPS and gellan likely reflect differences in their compositions. The CN32 EPS used in this study was not fractionated and thus contained a heterogeneous mixture of polysaccharides, proteins, lipids, and nucleic acids. The proteins and nucleic acids in EPS can bind strongly to iron oxides via phosphoryl groups (33, 39); therefore, strong preferential binding to lepidocrocite by multiple components of CN32 EPS is likely. Conversely, gellan is a highly purified EPS consisting primarily of a high-molecular-mass (~500 kDa) polysaccharide (additional details are provided in Supporting Information). Despite gellan’s high molecular mass, which should favor sorption, the overall charge density is relatively low, with only one carboxylate group per tetrasaccharide structural unit (~658 Da), which is likely to limit its competitive binding.

Our results offer new insight into factors that can contribute to green rust formation during iron oxide bioreduction; however, key questions remain. Although there are data for many of the anions examined in this study that indicate sorption to Fe(III) oxides occurs via formation of inner-sphere complexes (Table S2, Supporting Information); there is little known about the specific binding site(s) involved, particularly in the case of lepidocrocite. Likewise, the specific site(s) on lepidocrocite where electron transfer can occur are also not known. We are currently engaged in focused investigations probing the molecular-scale mechanism(s) of anion-specific controls on Fe(II) production kinetics and secondary mineralization product formation.

Environmental Implications. Iron biogeochemistry is complex and is coupled with the biogeochemical cycling of many major (C, S, N, O) and minor (e.g., P, As, and Se) elements. This, in turn, affects other biogeochemical processes, including contaminant fate and transport. Fe(II) is an effective reductant for a range of contaminants including chlorinated hydrocarbons, nitroaromatics, nitrate, Cr(VI), U(VI), Tc(VII), Np(V), and Pu(V). However, the redox reactivity

of Fe(II) depends strongly on its speciation. Among common Fe(II) phases, green rust is a particularly effective reductant for several contaminants of concern (40–43); therefore, an improved understanding of the processes leading to the formation of green rust in natural and engineered environments (e.g., *in situ* biostimulation of native populations of IRB for contaminant bioremediation) may lead to better management of contaminant fate and transport. Although our experimental conditions are not typical of natural environments (i.e., relatively high levels of electron donor (formate), Fe(III), and IRB), the formation of the green rust mineral fouggerite in reductomorphic soils correlates well with the activity of native IRB populations (44). Although the factors controlling the formation of fouggerite are not well-defined, our results suggest that oxyanions and various forms of NOM commonly found in soils and sediments, as well as the types and numbers bacterial cells and their exudates, may all play a role in the formation of fouggerite as a product of the bioreduction of Fe(III) oxides.

Acknowledgments

We thank Russell Cook for his assistance with SEM imaging; Michael McCormick for determining the surface area of the lepidocrocite used in this study; and Karen Haugen and three anonymous reviewers for their thoughtful reviews of the manuscript. Funding was provided by the U.S. Department of Energy's Office of Science (DOE-SC), Office of Biological and Environmental Research, Subsurface Biogeochemical Research Program, under contract DE-AC02-06CH11357. Use of the APS and the Electron Microscopy Center for Materials Research at Argonne National Laboratory was supported by the DOE-SC Office of Basic Energy Sciences, under contract DE-AC02-06CH11357. The submitted manuscript has been created by UChicago Argonne, LLC, Operator of Argonne National Laboratory ("Argonne"). Argonne, a U.S. Department of Energy Office of Science laboratory, is operated under Contract No. DE-AC02-06CH11357. The U.S. government retains for itself and others acting on its behalf, a paid-up, non-exclusive, irrevocable worldwide license in said article to reproduce, prepare derivative works, distribute copies to the public and perform publicly and display publicly, by or on behalf of the Government.

Supporting Information Available

Details on sources of chemicals; preparation of reagents; synthesis and characterization of lepidocrocite; measurement of Fe(II) concentrations; and characterization of secondary mineralization products by XRD, ^{57}Fe Mössbauer, and SEM. This material is available free of charge via the Internet at <http://pubs.acs.org>.

Literature Cited

- (1) Kukkadapu, R. K.; Zachara, J. M.; Fredrickson, J. K.; Kennedy, D. W. Biotransformation of two-line silica-ferrihydrite by a dissimilatory Fe(III)-reducing bacterium: Formation of carbonate green rust in the presence of phosphate. *Geochim. Cosmochim. Acta* **2004**, 68 (13), 2799–2814.
- (2) Fredrickson, J. K.; Zachara, J. M.; Kennedy, D. W.; Dong, H.; Onstott, T. C.; Hinman, N. W.; Li, S.-M. Biogenic iron mineralization accompanying the dissimilatory reduction of hydrous ferric oxide by a groundwater bacterium. *Geochim. Cosmochim. Acta* **1998**, 62 (19/20), 3239–3257.
- (3) Parmar, N.; Gorby, Y. A.; Beveridge, T. J.; Ferris, F. G. Formation of green rust and immobilization of nickel in response to bacterial reduction of hydrous ferric oxide. *Geomicrobiol. J.* **2001**, 18, 375–385.
- (4) Salas, E. C.; Berelson, W. M.; Hammond, D. E.; Kampf, A. R.; Nealson, K. H. The influence of carbon source on the products of dissimilatory iron reduction. *Geomicrobiol. J.* **2009**, 26, 451–462.
- (5) Glasauer, S.; Weidler, P. G.; Langley, S.; Beveridge, T. J. Controls on Fe reduction and mineral formation by a subsurface bacterium. *Geochim. Cosmochim. Acta* **2003**, 67 (7), 1277–1288.
- (6) O'Loughlin, E. J. Effects of electron transfer mediators on the biodegradation of lepidocrocite (γ -FeOOH) by *Shewanella putrefaciens* CN32. *Environ. Sci. Technol.* **2008**, 42 (18), 6876–6882.
- (7) O'Loughlin, E. J.; Larese-Casanova, P.; Scherer, M. M.; Cook, R. E. Green rust formation from the bioreduction of γ -FeOOH (lepidocrocite): Comparison of several *Shewanella* species. *Geomicrobiol. J.* **2007**, 24, 211–230.
- (8) Ona-Nguema, G.; Abdelmoula, M.; Jorand, F.; Benali, O.; Géhin, A.; Block, J.-C.; Génin, J.-M. R. Iron(II, III) hydroxycarbonate green rust formation and stabilization from lepidocrocite bioreduction. *Environ. Sci. Technol.* **2002**, 36 (1), 16–20.
- (9) Ona-Nguema, G.; Morin, G.; Wang, Y.; Menguy, N.; Juillot, F.; Olovi, L.; Aquilanti, G.; Abdelmoula, M.; Ruby, C.; Bargat, J. R.; Guyot, F.; Calas, G.; Brown, G. E., Jr. Arsenite sequestration at the surface of nano-Fe(OH)₂, ferrous-carbonate hydroxide, and green-rust after bioreduction of arsenic-sorbed lepidocrocite by *Shewanella putrefaciens*. *Geochim. Cosmochim. Acta* **2009**, 73, 1359–1381.
- (10) Jorand, F.; Zegeye, A.; Landry, F.; Ruby, C. Reduction of ferric green rust by *Shewanella putrefaciens*. *Lett. Appl. Microbiol.* **2007**, 45, 515–521.
- (11) Zegeye, A.; Ruby, C.; Jorand, F. Kinetic and thermodynamic analysis during dissimilatory γ -FeOOH reduction: Formation of green rust I and magnetite. *Geomicrobiol. J.* **2007**, 24, 51–64.
- (12) Hansel, C. M.; Benner, S. G.; Neiss, J.; Dohnalkova, A.; Kukkadapu, R. K.; Fendorf, S. Secondary mineralization pathways induced by dissimilatory iron reduction of ferrihydrite under advective flow. *Geochim. Cosmochim. Acta* **2003**, 67 (16), 2977–2992.
- (13) Borch, T.; Masue, Y.; Kukkadapu, R. K.; Fendorf, S. Phosphate imposed limitations on biological reduction and alteration of ferrihydrite. *Environ. Sci. Technol.* **2007**, 41 (1), 166–172.
- (14) Bearcock, J. M.; Perkins, W. T.; Dinelli, E.; Wade, S. C. Fe(II)/Fe(III) 'green rust' developed within ocherous coal mine drainage sediment in South Wales, U.K. *Mineral. Mag.* **2006**, 70 (6), 731–741.
- (15) Christiansen, B. C.; Balic-Zunic, T.; Dideriksen, K.; Stipp, S. L. S. Identification of green rust in groundwater. *Environ. Sci. Technol.* **2009**, 43 (10), 3436–3441.
- (16) Feder, F.; Trolard, F.; Klingelhöfer, G.; Bourrié, G. In situ Mössbauer spectroscopy: Evidence for green rust (fouggerite) in a gleysoil and its mineralogical transformations with time and depth. *Geochim. Cosmochim. Acta* **2005**, 69 (18), 4463–4483.
- (17) Génin, J.-M. R.; Bourrié, G.; Trolard, F.; Abdelmoula, M.; Jaffrezic, A.; Refait, P.; Maitre, V.; Humbert, B.; Herbillon, A. Thermodynamic equilibria in aqueous suspensions of synthetic and natural Fe(II)-Fe(III) green rusts: Occurrences of the mineral in hydromorphic soils. *Environ. Sci. Technol.* **1998**, 32 (8), 1058–1068.
- (18) Root, R. A.; Dixit, S.; Campbell, K. M.; Jew, A. D.; Hering, J. G.; O'Day, P. A. Arsenic sequestration by sorption processes in high-iron sediments. *Geochim. Cosmochim. Acta* **2007**, 71, 5782–5803.
- (19) Dong, H.; Fredrickson, J. K.; Kennedy, D. W.; Zachara, J. M.; Kukkadapu, R. K.; Onstott, T. C. Mineral transformation associated with the microbial reduction of magnetite. *Chem. Geol.* **2000**, 169, 299–318.
- (20) Fredrickson, J. K.; Kota, S.; Kukkadapu, R. K.; Liu, C.; Zachara, J. M. Influence of electron donor/acceptor concentrations on hydrous ferric oxide (HFO) bioreduction. *Biodegradation* **2003**, 14, 91–103.
- (21) Johnson, C. M.; Roden, E. E.; Welch, S. A.; Beard, B. L. Experimental constraints on Fe isotope fractionation during magnetite and Fe carbonate formation coupled to dissimilatory hydrous ferric oxide reduction. *Geochim. Cosmochim. Acta* **2005**, 69 (4), 963–993.
- (22) Zachara, J. M.; Fredrickson, J. K.; Li, S.-M.; Kennedy, D. W.; Smith, S. C.; Gassman, P. L. Bacterial reduction of crystalline Fe³⁺ oxides in single phase suspension and subsurface materials. *Am. Mineral.* **1998**, 83, 1426–1443.
- (23) Zachara, J. M.; Kukkadapu, R. K.; Frederickson, J. K.; Gorby, Y. A.; Smith, S. C. Biomimetic mineralization of poorly crystalline Fe(III) oxides by dissimilatory metal reducing bacteria (DMRB). *Geomicrobiol. J.* **2002**, 19, 179–207.
- (24) Cornell, R. M.; Schwertmann, U. *The Iron Oxides: Structure, Properties, Reactions, Occurrence and Uses*, 2nd ed.; Wiley-VCH: New York, 2003; p 664.
- (25) Behrends, T.; Van Cappellen, P. Transformation of hematite into magnetite during dissimilatory iron reduction—Conditions and mechanisms. *Geomicrobiol. J.* **2007**, 24, 403–416.

- (26) Kukkadapu, R. K.; Zachara, J. M.; Fredrickson, J. K.; Kennedy, D. W.; Dohnalkova, A. C.; McCready, D. E. Ferrous hydroxy carbonate is a stable transformation product of biogenic magnetite. *Am. Mineral.* **2005**, *90*, 510–515.
- (27) Roh, Y.; Zhang, C.-L.; Vali, H.; Lauf, R. J.; Zhou, J.; Phelps, T. J. Biogeochemical and environmental factors in Fe biomimetic mineralization: Magnetite and siderite formation. *Clays Clay Miner.* **2003**, *51* (1), 83–95.
- (28) Sparks, N. H. C.; Mann, S.; Bazylinski, D. A.; Lovley, D. R.; Jannasch, H. W.; Frankel, R. B. Structure and morphology of magnetite anaerobically-produced by a marine magnetotactic bacterium and a dissimilatory iron-reducing bacterium. *Earth Planet. Sci. Lett.* **1990**, *98*, 14–22.
- (29) Biber, M.; dos Santos Afonso, M.; Stumm, W. The coordination chemistry of weathering: IV. Inhibition of the dissolution of oxide minerals. *Geochim. Cosmochim. Acta* **1994**, *58* (9), 1999–2010.
- (30) Liu, C.; Zachara, J. M.; Foster, N. S.; Strickland, J. Kinetics of reductive dissolution of hematite by bioreduced anthraquinone-2,6-disulfonate. *Environ. Sci. Technol.* **2007**, *41* (22), 7730–7735.
- (31) Drits, V. A.; Sokolova, T. N.; Sokolova, G. V.; Cherkashin, V. I. New members of the hydrotalcite-manasseite group. *Clays Clay Miner.* **1987**, *35* (6), 401–417.
- (32) Kostka, J. E.; Nealson, K. H. Dissolution and reduction of magnetite by bacteria. *Environ. Sci. Technol.* **1995**, *29* (10), 2535–2540.
- (33) Parikh, S. J.; Chorover, J. ATR-FTIR spectroscopy reveals bond formation during bacterial adhesion to iron oxide. *Langmuir* **2006**, *22*, 8492–8500.
- (34) Lower, B. H.; Shi, L.; Youngsunthon, R.; Droubay, T. C.; McCready, D. E.; Lower, S. K. Specific bonds between an iron oxide surface and outer membrane cytochromes MtrC and OmcA from *Shewanella oneidensis* MR-1. *J. Bacteriol.* **2007**, *189* (13), 4944–4952.
- (35) Xiong, Y.; Shi, L.; Chen, B.; Mayer, M. U.; Lower, B. H.; Londer, Y.; Bose, S.; Hochella, M. F.; Fredrickson, J. K.; Squier, T. C. High-affinity binding and direct electron transfer to solid metals by the *Shewanella oneidensis* MR-1 outer membrane c-type cytochrome OmcA. *J. Am. Chem. Soc.* **2006**, *128*, 13978–13979.
- (36) Goldberg, S. Reactions of boron with soils. *Plant Soil* **1997**, *193*, 35–48.
- (37) Johnson, S. E.; Loepert, R. H. Role of organic acids in phosphate mobilization from iron oxide. *Soil Sci. Soc. Am. J.* **2006**, *70*, 222–234.
- (38) Mohapatra, D.; Singh, P.; Zhang, W.; Pullammanappallil, P. The effect of citrate, oxalate, acetate, silicate and phosphate on stability of synthetic arsenic-loaded ferrihydrite and Al-ferrihydrite. *J. Hazard. Mater.* **2005**, *B124*, 95–100.
- (39) Omoike, A.; Chorover, J. Adsorption to goethite of extracellular polymeric substances from *Bacillus subtilis*. *Geochim. Cosmochim. Acta* **2006**, *70*, 827–838.
- (40) Elsner, M.; Schwarzenbach, R. P.; Haderlein, S. B. Reactivity of Fe(II)-bearing minerals toward reductive transformation of organic contaminants. *Environ. Sci. Technol.* **2004**, *38* (3), 799–807.
- (41) Lee, W.; Batchelor, B. Reductive capacity of natural reductants. *Environ. Sci. Technol.* **2003**, *37* (3), 535–541.
- (42) O'Loughlin, E. J.; Kelly, S. D.; Kemner, K. M. XAFS investigation of the interactions of UVⁱI with secondary mineralization products from the bioreduction of Fe^{III} oxides. *Environ. Sci. Technol.* **2010**, *44* (5), 1656–1661.
- (43) Williams, A. G. B.; Scherer, M. M. Kinetics of Cr(VI) reduction by carbonate green rust. *Environ. Sci. Technol.* **2001**, *35*, 3488–3494.
- (44) Berthelin, J.; Oma-Nguema, G.; Stemmler, S.; Quantin, C.; Abdelmoula, M.; Jorand, F. Bioreduction of ferric species and biogenesis of green rusts in soils. *C. R. Geosci.* **2006**, *338*, 447–455.

ES100294W

Supporting Information

Effects of oxyanions, natural organic matter, and bacterial cell numbers on the bioreduction of lepidocrocite (γ -FeOOH) and the formation of secondary mineralization products

Edward J. O'Loughlin^{1*}, Christopher A. Gorski², Michelle M. Scherer², Maxim I. Boyanov¹, and Kenneth M. Kemner¹

¹*Biosciences Division, Argonne National Laboratory, Argonne, IL 60439-4843*

²*Department of Civil and Environmental Engineering, University of Iowa, Iowa City, IA 52242-1527*

*Corresponding author: Biosciences Division, Argonne National Laboratory, Building 203, Room E-137,
9700 South Cass Ave., Argonne, IL, 60439-4843, USA; e-mail address: oloughlin@anl.gov;
telephone: 630-252-9902; fax: 630-252-9793

Pages 21

Tables 3

Figures 13

ADDITIONAL INFORMATION FOR THE EXPERIMENTAL SECTION

Chemicals. Unless otherwise indicated, all chemicals were of reagent grade or higher purity and were obtained from commercial sources (Sigma-Aldrich, Fisher Scientific, and Fluka). Lepidocrocite (γ -FeOOH) was synthesized by air oxidation of a ferrous chloride solution using a modified version of the procedure in Schwertmann and Cornell (2000). Briefly, 30 g of $\text{FeCl}_2 \cdot 4\text{H}_2\text{O}$ was dissolved in 900 mL of water, and the resulting solution was filtered through a 0.2- μm nylon filter to remove any Fe(III) solids present. The pH of the solution was adjusted to 6.0 with 0.5 M NaOH, and the resulting blue/green suspension was sparged with air. The suspension was maintained at pH 5.5–6.0 by titration with 0.5 M NaOH until the addition of base was no longer needed (~ 1.5 h). The solids were repeatedly washed by centrifugation and resuspension in distilled water, then dried at 60 °C and ground to pass a 200-mesh sieve. The solids consisted of highly crystalline lepidocrocite, as determined by powder X-ray diffraction (Figure S1), exhibiting the elongated, lath-like morphology typical of lepidocrocite (Figure S2). The specific surface area was $73.13 \pm 0.76 \text{ m}^2 \text{ g}^{-1}$ as determined by multipoint B.E.T. analysis of N_2 adsorption using a Micrometrics Tristar II Surface Area Analyzer.

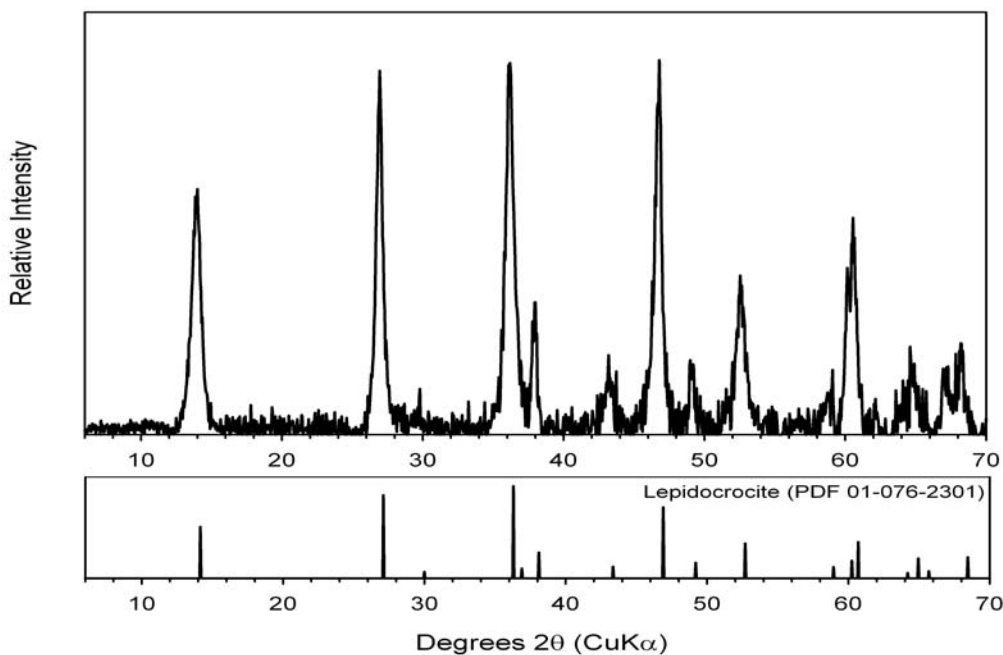


Figure S1. XRD analysis of the lepidocrocite used in this study.

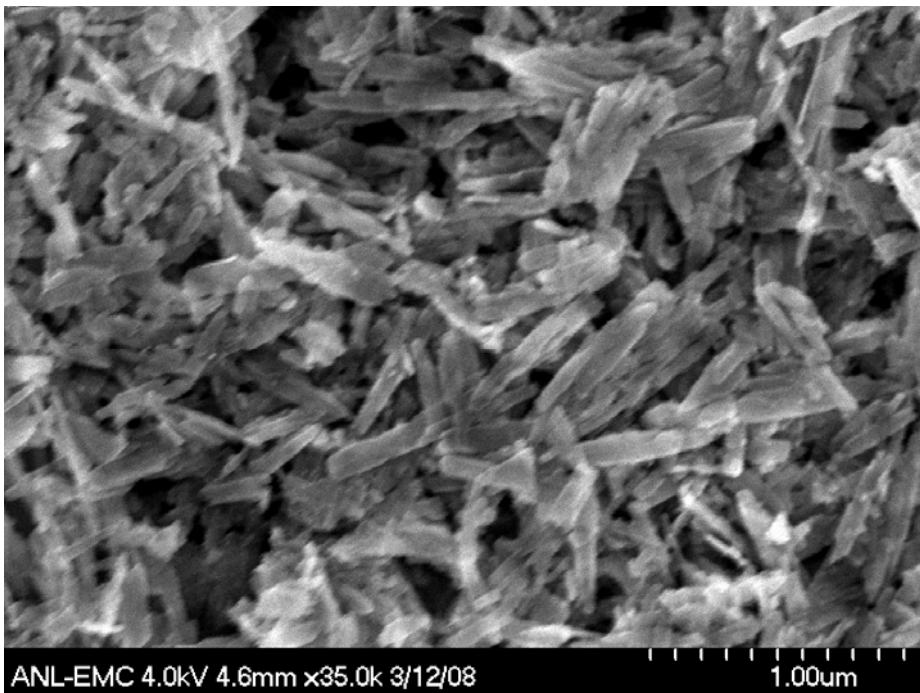


Figure S2. SEM image of the lepidocrocite used in this study.

Extracellular polymeric substances (EPS)—heterogeneous mixtures of biopolymers composed of proteins, polysaccharides, lipids, and nucleic acids—were isolated from cultures of *Shewanella putrefaciens* CN32 (ATCC BAA-453) using an approach modified from Omoike and Chorover (2006). Briefly, *S. putrefaciens* CN32 was cultured aerobically on tryptic soy broth at ~22 °C and 60 rpm on an orbital shaker until early stationary growth phase was reached (~ 24 h). The cells were removed by centrifugation at 15,300 × g for 30 min at 4 °C. The EPS (hereafter designated CN32 EPS) was precipitated from the supernatant solution by adding cold acetone at a volumetric ratio of 3:1 (acetone:supernatant). The precipitated EPS was separated by centrifugation at 15,300 × g for 10 min at 4 °C, washed twice with cold acetone, and dried at 30 °C.

Gellan is nominally an extracellular, high-molecular-weight (~500 kDa) polysaccharide produced by the bacterium *Sphingomonas elodea* (Kang et al. 1982). The polymer is composed of a repeating tetrasaccharide unit that consists of two residues of D-glucose, one L-rhamnose residue, and one D-glucuronic acid residue, with the following structure (Jansson et al. 1983):



Gellan was purchased from Sigma under the trade name Phytigel and prepared as a sodium salt, as described by Doner and Douds (1995).

Leonardite humic acid (LHA, 1S104H), Pony Lake fulvic acid (PLFA, 1R109F), Elliott soil humic acid (ESHA, 1S102H), Suwannee River fulvic acid (SRFA, 2S101F), and Suwannee River humic acid (SRHA, 2S101H) were purchased from the International Humic Substance Society (<http://www.ihss.gatech.edu/>). The aromaticities and molecular weights of the humic substances are provided in Table S1. LHA, ESHA, SRFA, and SRHA are derived primarily from the degradation of terrestrial plants and thus contain a significant fraction of lignin residues, resulting in relatively high aromatic C contents. PLFA was isolated from a coastal pond in Antarctica which does not receive inputs of terrestrial-plant-derived C; therefore, PLFA is derived primarily from the degradation of microbially produced polypeptides and polysaccharides (Mao et al. 2007).

Table S1. Aromaticity and molecular weight of the humic substances used in this study.

Humic Substance	$^{13}\text{C} f_a$	Aromaticity ^a	Weight-Average Molecular Weight ^b (Da)
Elliott soil humic acid (ESHA)	0.50	6202 ^c	
Leonardite humic acid (LHA)	0.58	5867 ^c	
Pony Lake fulvic acid (PLFA)	0.13	1450 ^d	
Sewanee River fulvic acid (SRFA)	0.30	2519 ^e	
Sewanee River humic acid (SRHA)	0.37	2831 ^e	

^a Thorn and Cox, 2009.

^b Determined by HPSEC using the method of Chin et al., 1994.

^c Karanfil et al., 1996.

^d Mao et al., 2007.

^e O'Loughlin et al., 2000.

Individual stock solutions containing 100 mM citrate, oxalate, or phosphate; 10 mM arsenate (Na_2HAsO_4), borate (H_3BO_3), molybdate (Na_2MoO_4), silicate (Na_2SiO_3), or tungstate (Na_2WO_4); 2 g L⁻¹ of LHA, PLFA, SHA, SRFA, or SRHA; or 200 mg L⁻¹ of CN32 EPS or gellan were prepared in water (with 1 M NaOH added as needed to facilitate the dissolution of the humic acids), adjusted to pH 7.5, and filter-sterilized (0.22 μm).

Analytical Methods. The reduction of lepidocrocite was monitored by measuring the Fe(II) content of 0.75 M HCl extracts of the suspensions [referred to hereafter as total Fe(II)]. Samples for Fe(II) analysis were prepared by adding 0.75 mL of anoxic 1 M HCl to 0.25 mL of suspension. The samples were mixed on an end-over-end shaker for two weeks, and then centrifuged at 25,000 $\times g$ for 10 min. The Fe(II) concentrations in the supernatants were determined by the ferrozine assay (Stookey 1970). Briefly, 1 mL of HEPES-buffered ferrozine reagent (Sørensen 1982) was added to 50 μL of supernatant, and the absorbance at 562 nm was measured. Total As, B, Mo, P, Si, and W concentrations in solution were measured by inductively coupled plasma-optical emission spectroscopy using a PerkinElmer 4300DV instrument. Solution concentrations of citrate and oxalate were measured with an Agilent 1100 series HPLC equipped with an ultraviolet absorbance detector. Each sample was diluted with an equal volume of 10 mM H₂SO₄, and 50 μL of the diluted sample was injected onto a Bio-Rad Aminex HPX-87H ion-exchange column (7.8 \times 300 mm). The column was eluted with 5 mM H₂SO₄ at a flow rate of 0.6 mL min⁻¹ at 50 °C, with analyte detection at 210 nm.

The secondary mineralization products were analyzed by X-ray diffractions (XRD) with a Rigaku MiniFlex X-ray diffractometer with Ni-filtered Cu K_α radiation. Samples for XRD analysis were collected by filtration on 25-mm, 0.22- μm nylon filters and covered with 8.4- μm -thick Kapton® film under anoxic conditions; although the XRD analysis was conducted under ambient atmosphere, samples prepared in this manner showed no evidence of oxidation when scanned between 5° and 80° 2θ at a speed of 1.25° 2θ min⁻¹ (samples containing green rust) or 0.35° 2θ min⁻¹ (samples containing magnetite/FHC).

The XRD patterns were analyzed with the JADE 7 software package (MDI, Livermore, CA) to remove the background through polynomial fitting and also to remove the $K_{\alpha 2}$ components.

Samples for scanning electron microscopy (SEM) imaging were prepared by placing 500 μ L of suspension on aluminum specimen mounts, allowing the solids to settle, removing the overlying liquid with a pipette, and drying the film of solids in a glove box. Specimens were briefly (< 30 s) exposed to air during transfer to the Hitachi S-4700-II FEG-SEM.

Transmission Mössbauer spectroscopy was performed with a variable-temperature He-cooled system with a 1024-channel detector. The ^{57}Co source used (~50 mCi) was in a Rh matrix at room temperature. All center shifts reported are relative to α -Fe foil at room temperature. Samples were prepared by filtering the cell suspension (approx. 4 mL) in an anaerobic glove box with recoverable filter paper. The filter paper was then sealed between two pieces of 5 mm Kapton tape to avoid oxidation while the sample was mounted. No indication of inadvertent oxidation was observed.

Spectral fitting was done using Recoil Software (University of Ottawa, Ottawa, Canada). Voigt-based fitting was used to model the spectra to determine the hyperfine parameters and the relative areas between phases. The Lorentzian linewidth was held at 0.12 mm s^{-1} , as it was the linewidth measured on the spectrometer for an ideally thick α -Fe foil. The relative peak areas (1:1 for doublets, 3:2:1:1:2:3 for sextets) were held constant throughout fitting. Each phase was fitted with only a single component (i.e., multiple QS and H distributions were not allowed for a single phase in fitting). Spectra that contained ordered ferrous hydroxy carbonate (FHC) (e.g., Figure 3, bottom right spectrum) could not be fit because the dependence of the observed phases on the initial assumed values made it impossible to determine which model was correct. These spectra were qualitatively consistent with those collected at other temperatures.

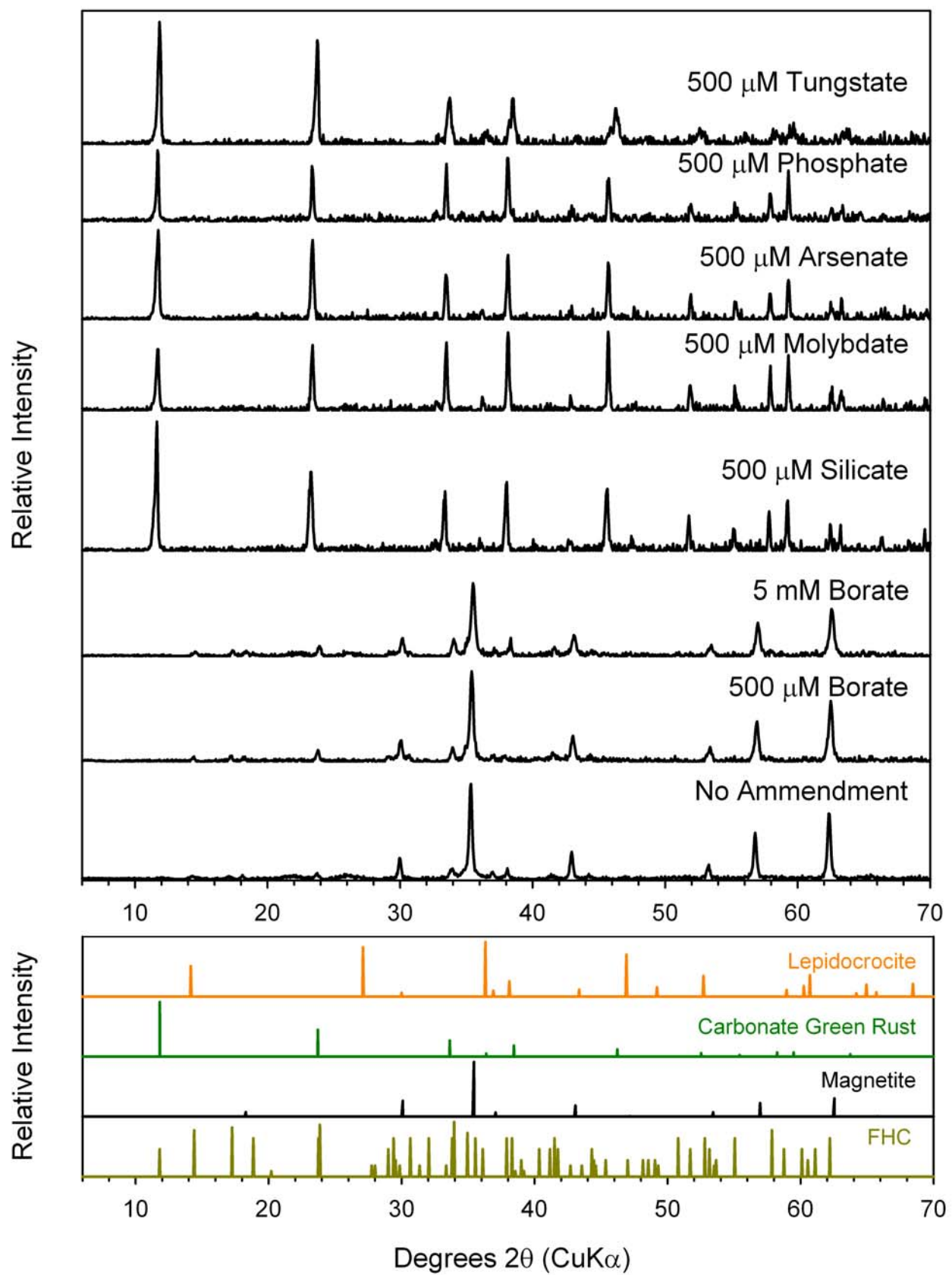


Figure S3. XRD analysis of the solids in the unamended control and oxyanion-amended systems.

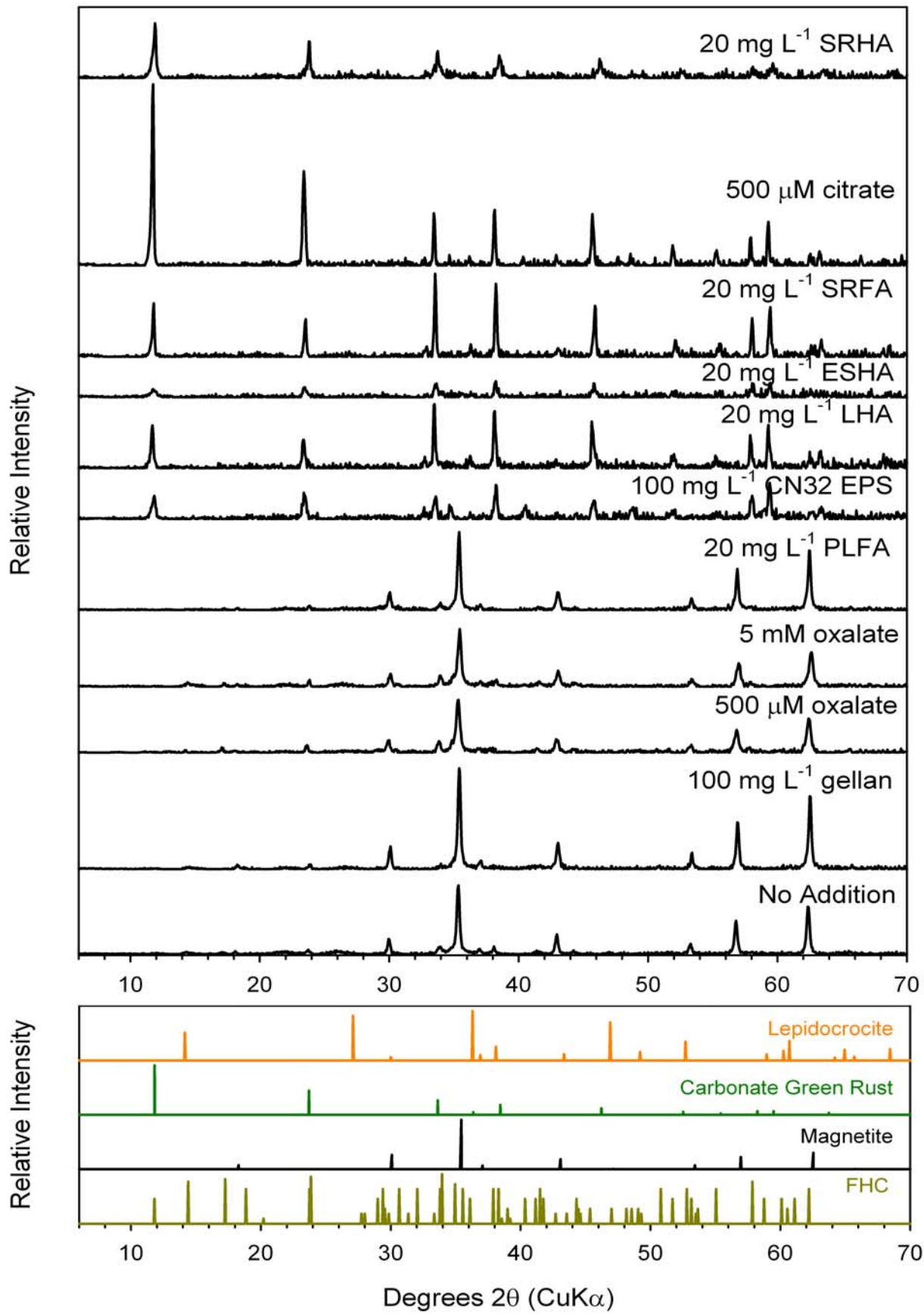


Figure S4. XRD analysis of the solids in the unamended control and systems amended with natural organic matter.

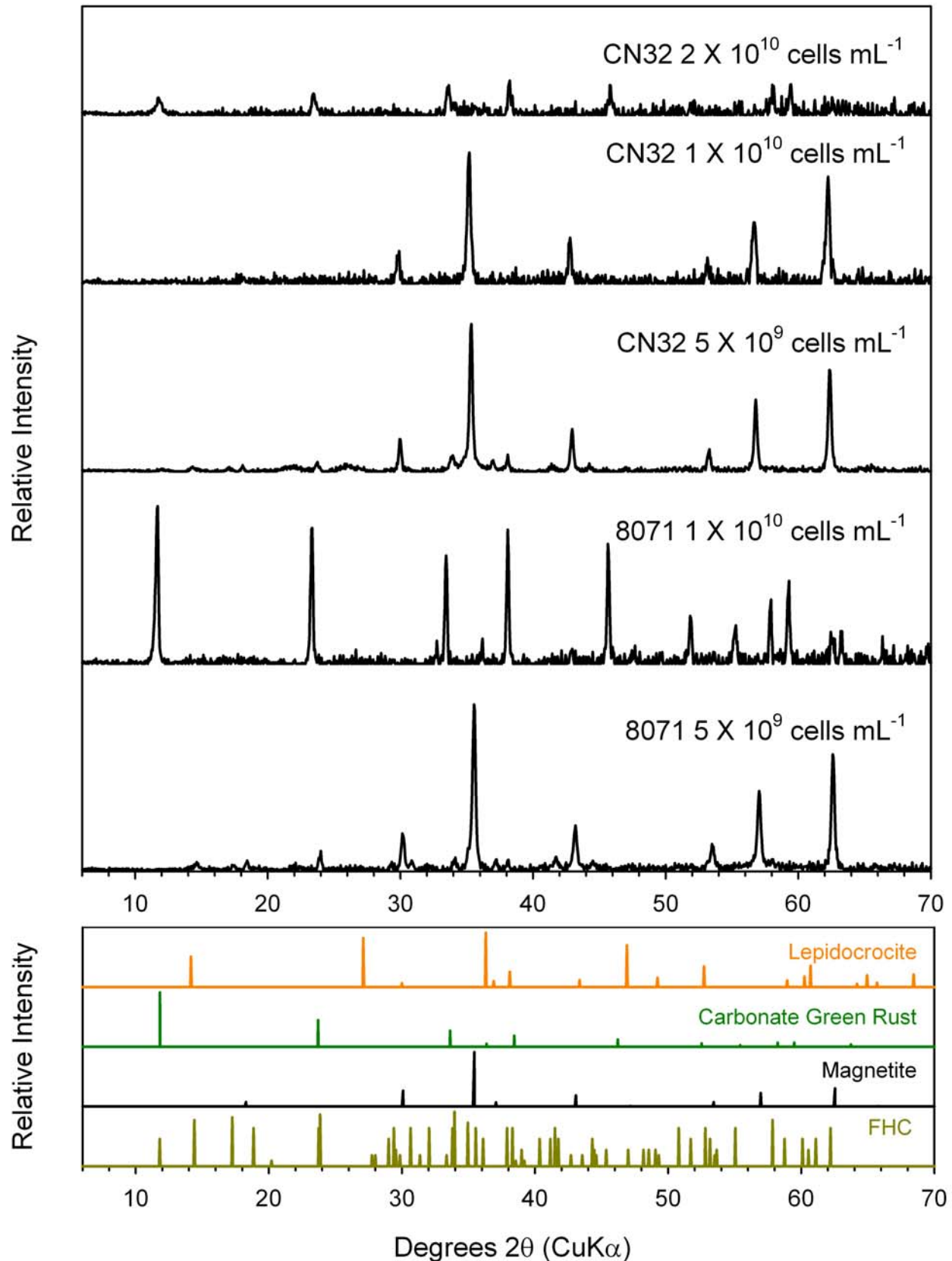


Figure S5. XRD analysis of the solids in systems containing various cell densities of *S. putrefaciens* strains CN32 and ATCC 8071.

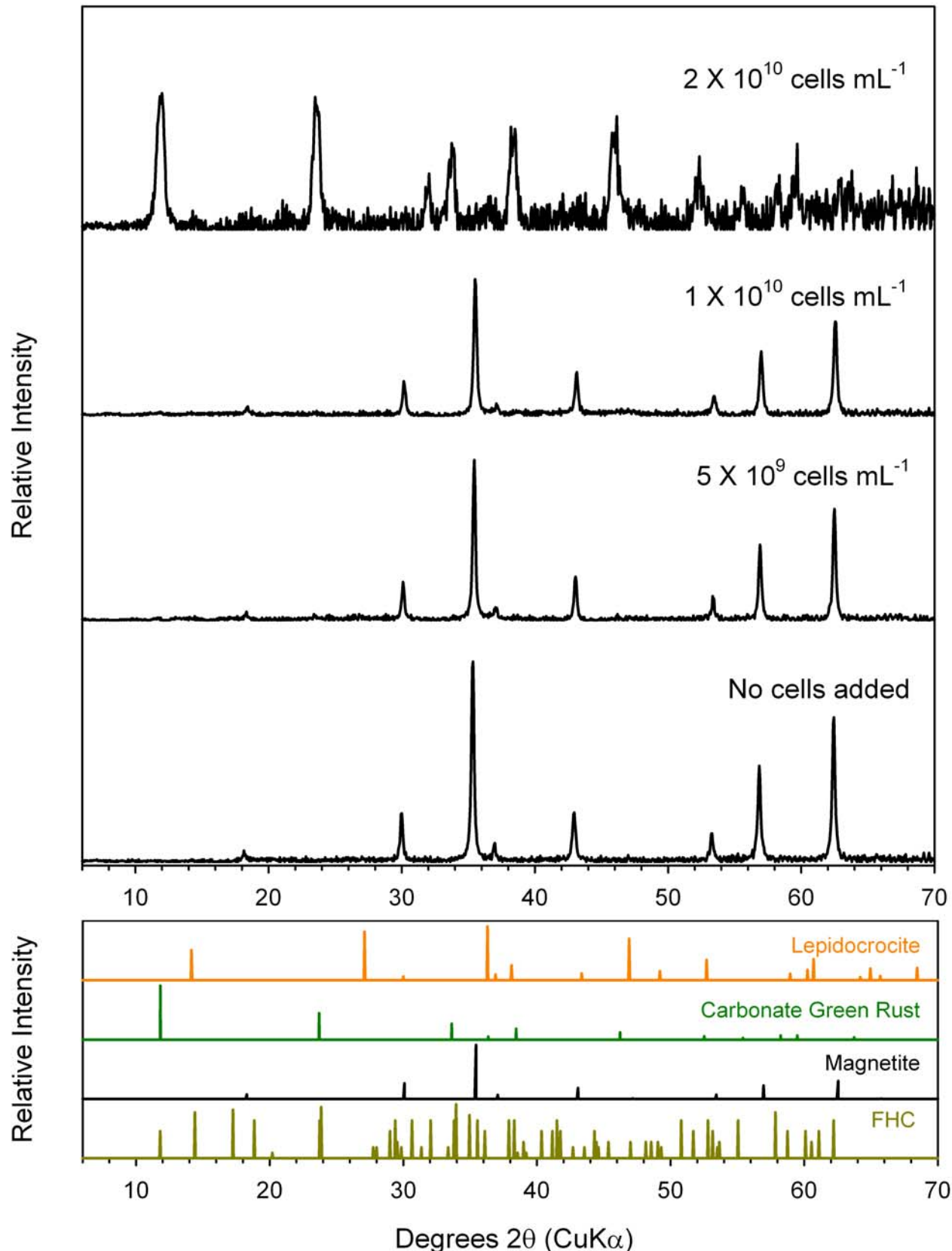


Figure S6. XRD analysis of the solids formed from the abiotic reduction of lepidocrocite by Pd/H₂/AQDS in the presence of various amounts of pasteurized *S. putrefaciens* CN32 cells.

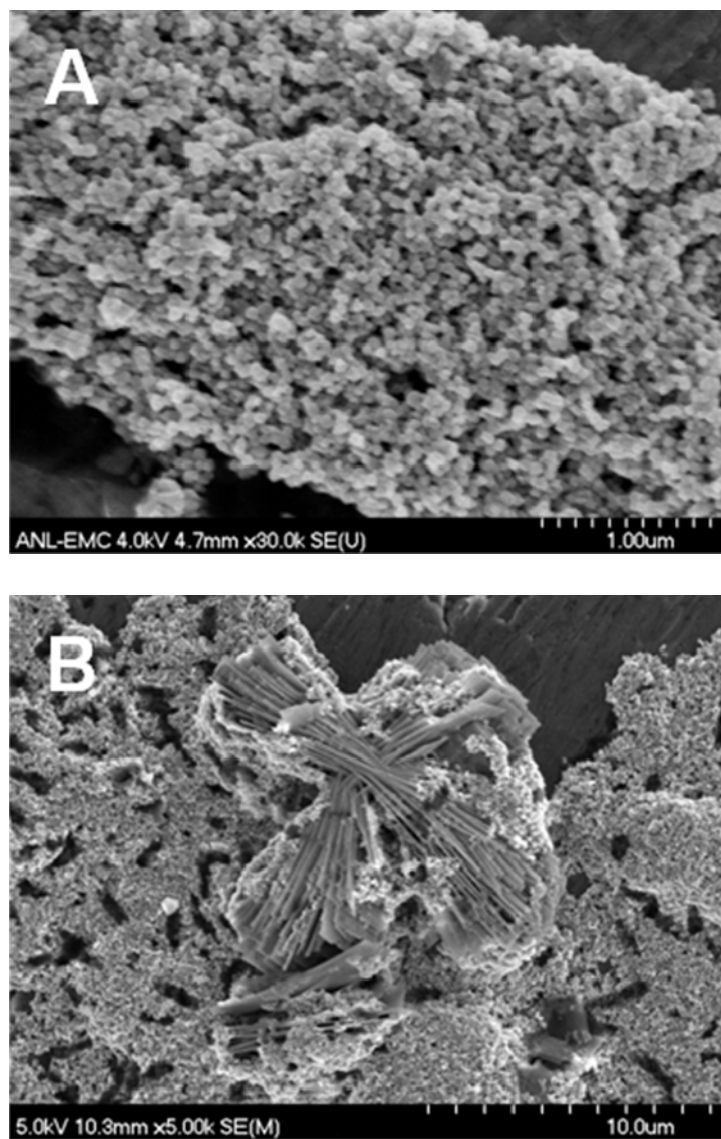


Figure S7. SEM images of secondary mineralization products formed in the absence of amendments: magnetite (A) and magnetite and FHC (B).

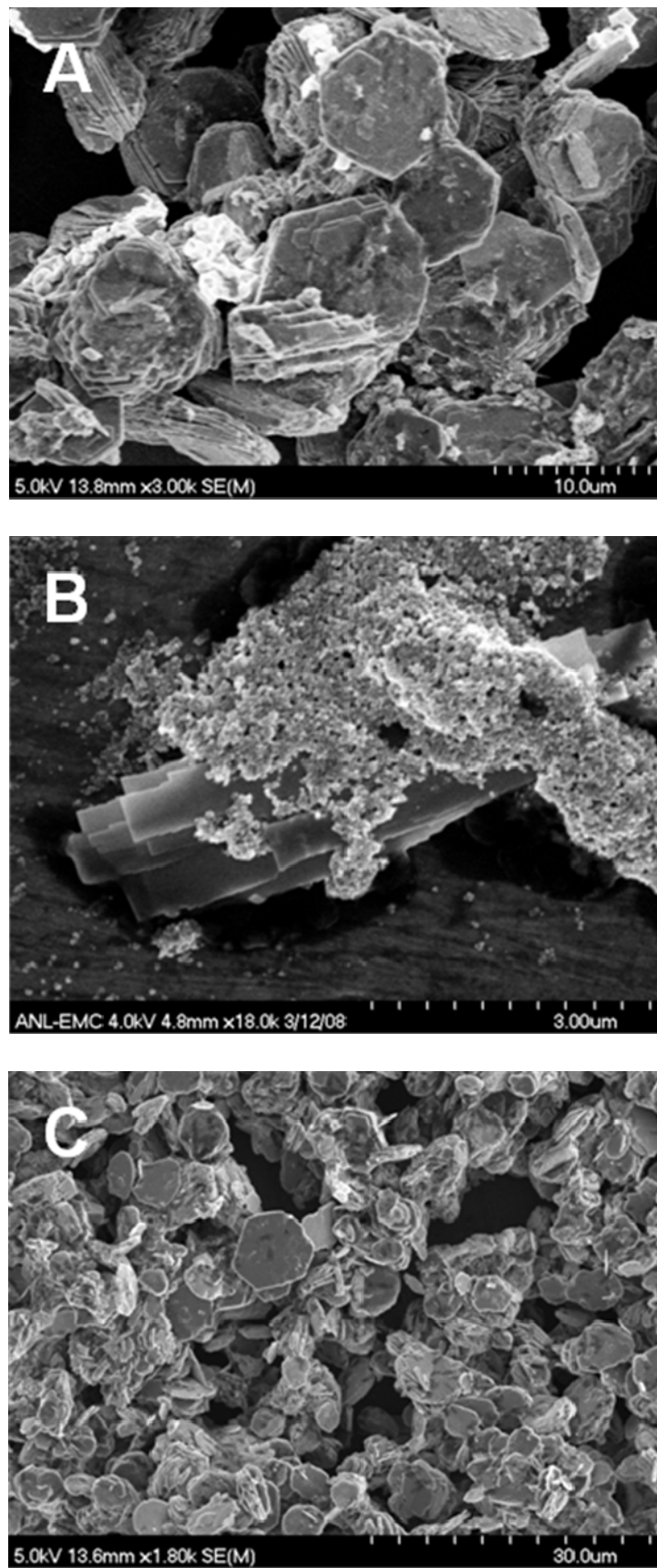


Figure S8. SEM images of secondary mineralization products formed in the presence of 500 μ M arsenate (A), 500 μ M borate (B), and 500 μ M molybdenum (C).

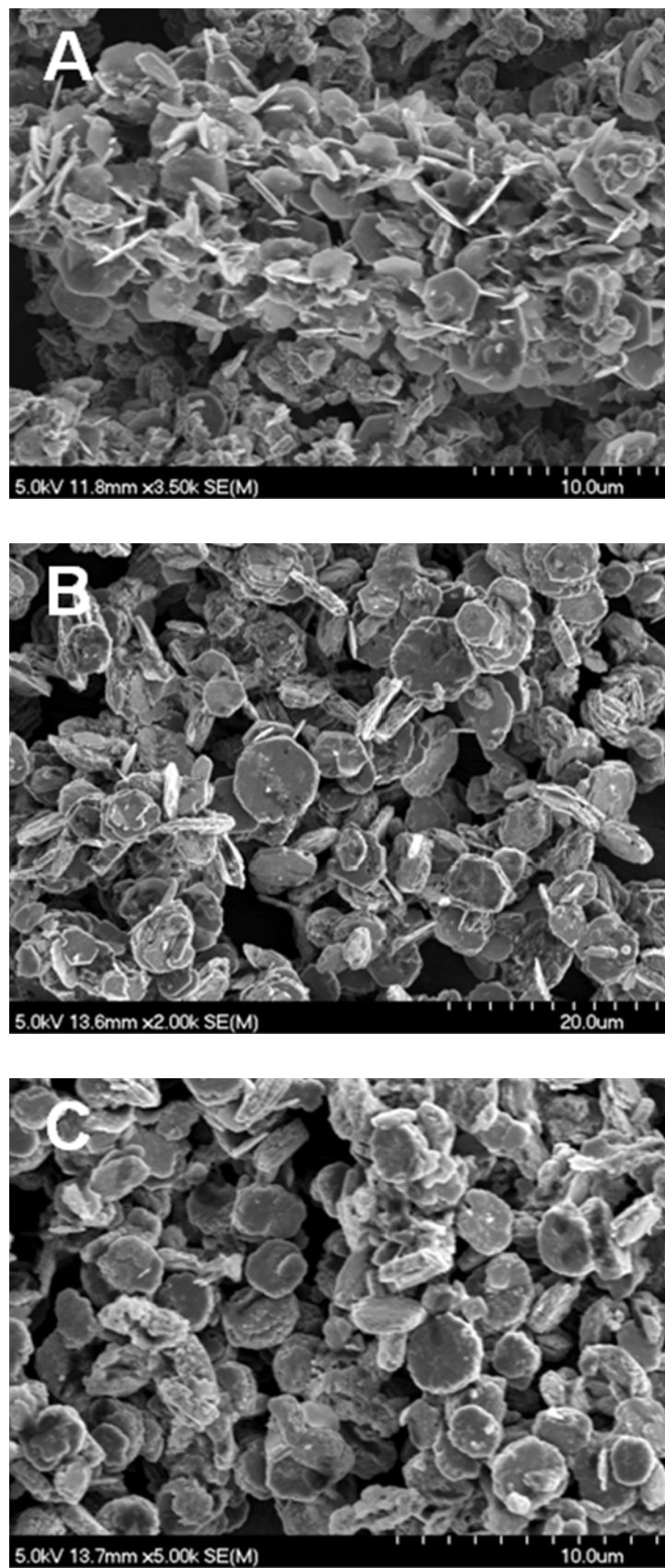


Figure S9. SEM images of secondary mineralization products formed in the presence of 500 μM phosphate (A), 500 μM silicate (B), and 500 μM tungstate (C).

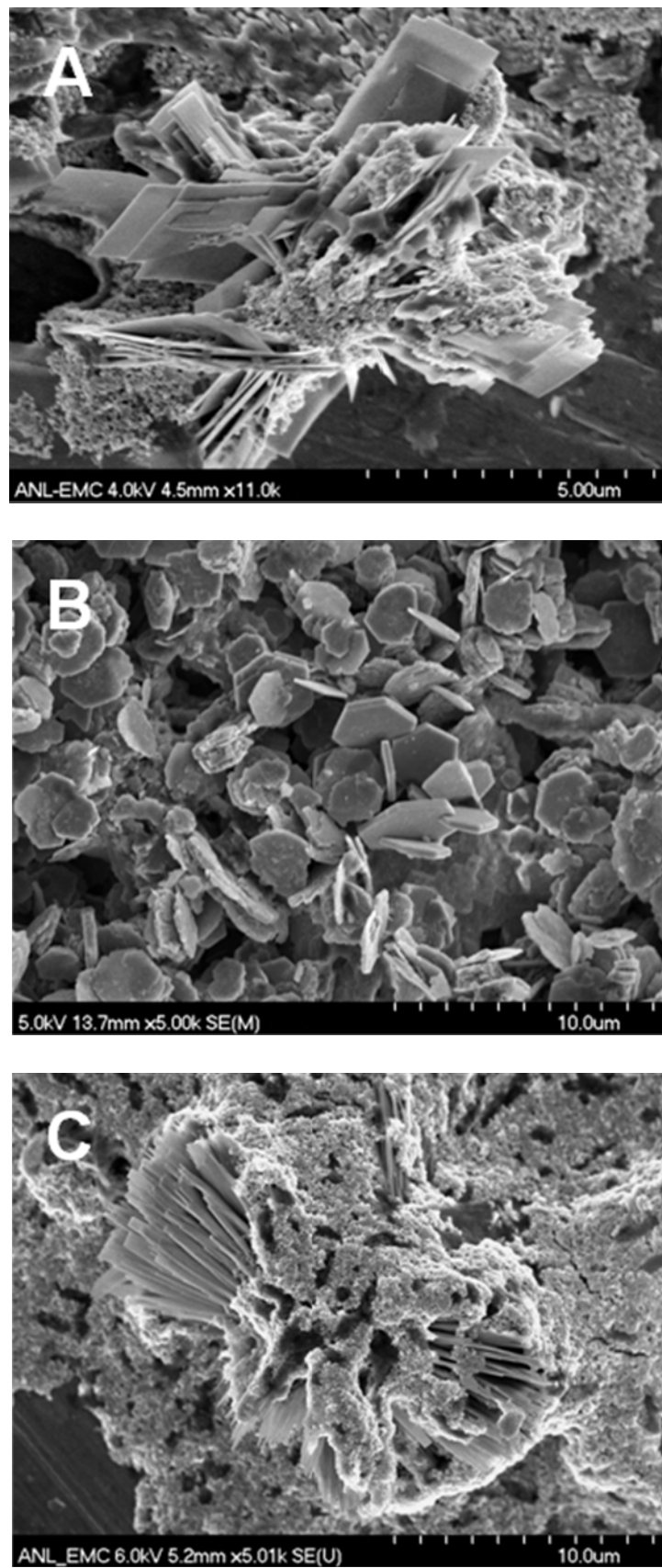


Figure S10. SEM images of secondary mineralization products formed in the presence of 500 μM oxalate (A), 500 μM citrate (B), and 20 mg L⁻¹ of Pony Lake fulvic acid (C).

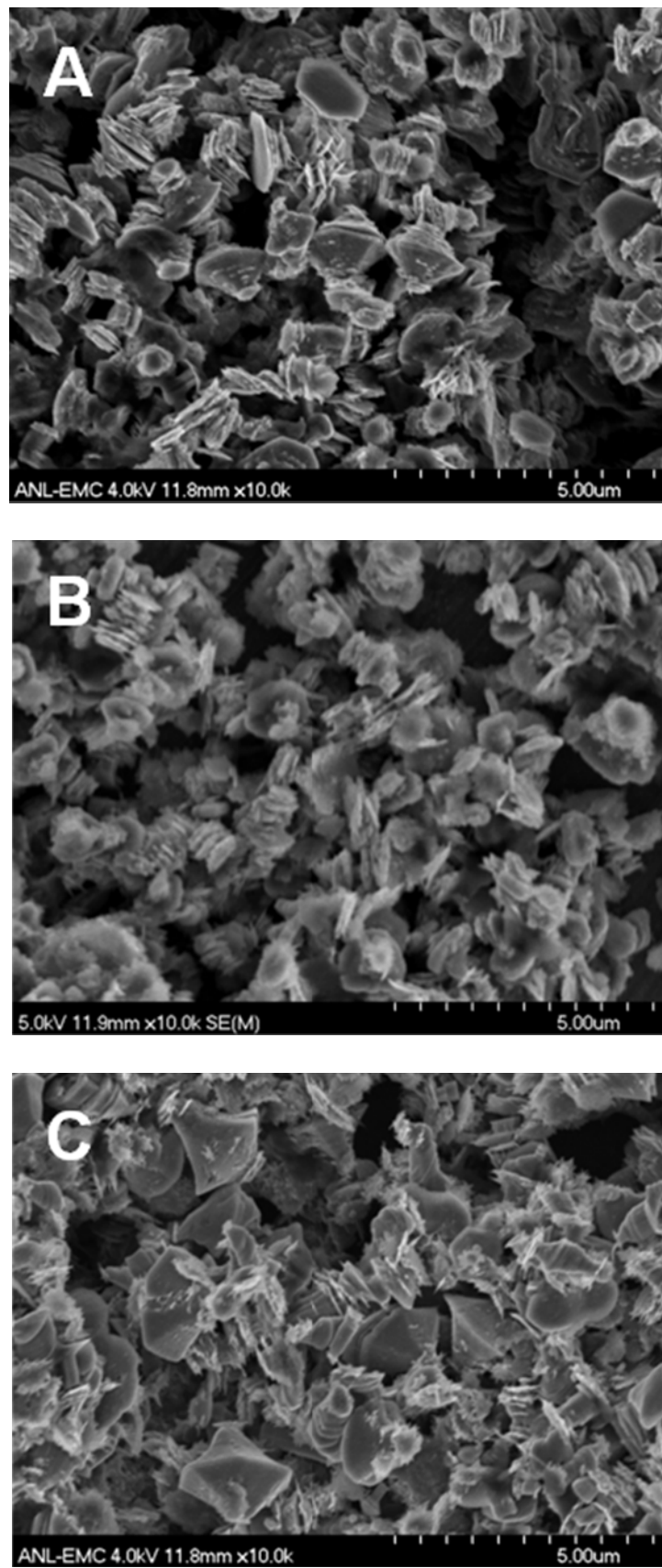


Figure S11. SEM images of products formed in the presence of (A) leonardite humic acid (20 mg L^{-1}), (B) Suwannee River humic acid (20 mg L^{-1}), and (C) Suwannee River fulvic acid (20 mg L^{-1}).

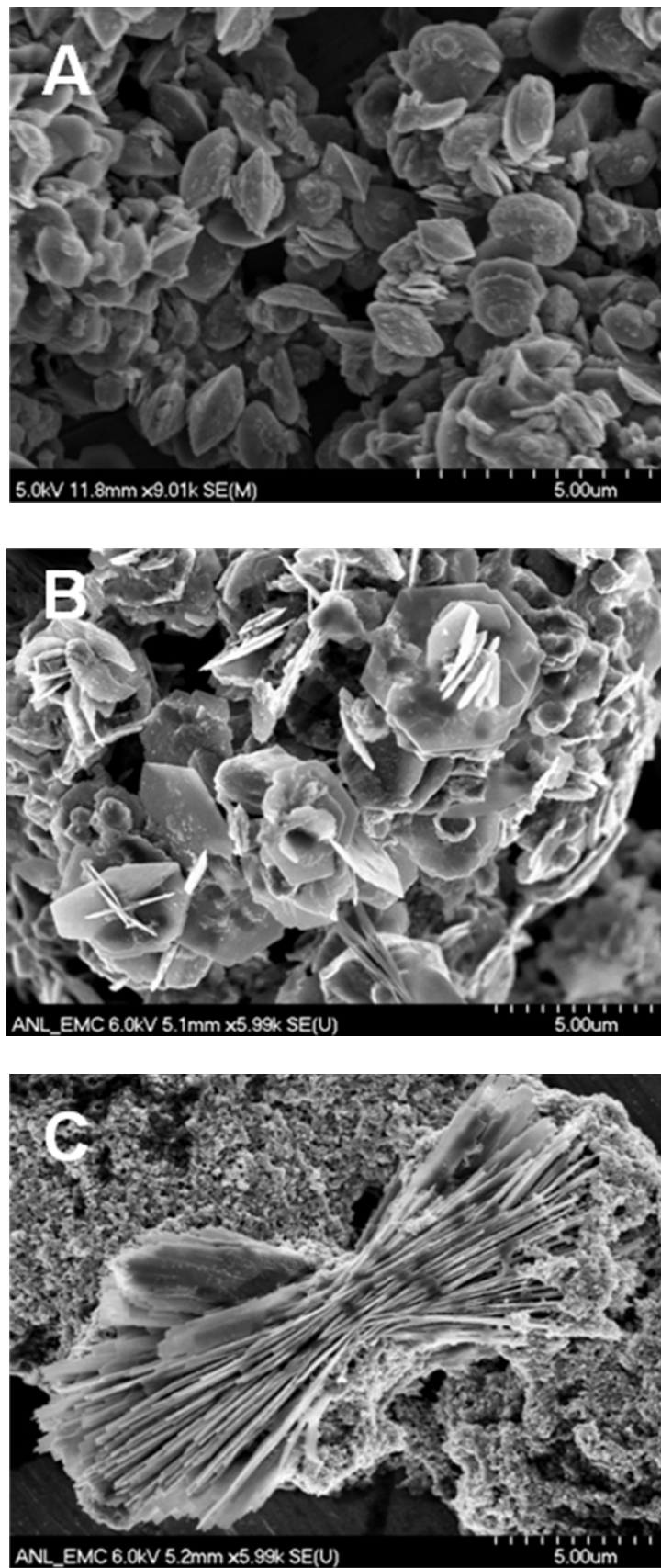


Figure S12. SEM images of products formed in the presence of (A) Elliott soil humic acid (20 mg L^{-1}), (B) EPS from *S. putrefaciens* CN32 (100 mg L^{-1}), and (C) gellan (100 mg L^{-1}).

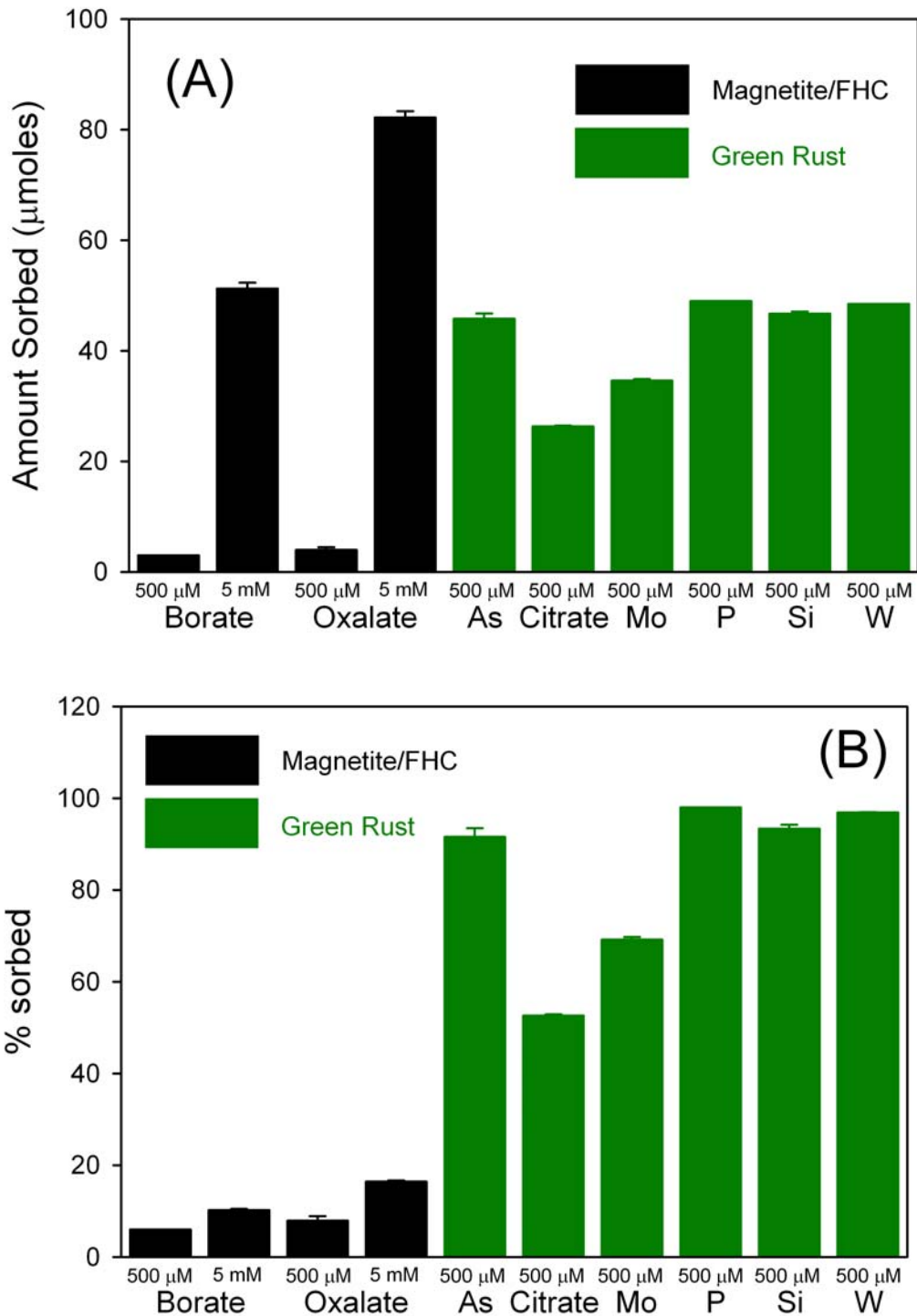


Figure S13. Uptake of inorganic oxyanions, oxalate, and citrate by lepidocrocite prior to inoculation in terms of μmols sorbed (A) and % sorbed (B). The color of the bar indicates the dominant secondary mineralization product formed in each system.

Table S2. Overview of literature on arsenate, borate, citrate, molybdate, oxalate, phosphate, silicate, and tungstate adsorption to lepidocrocite (if data are available) or to other iron(III) oxides.

Ligand	Iron oxide	pH	Surface Complex	Analytical Approach/Method ^a	Reference
Arsenate	goethite hydrated goethite hydrated ferric oxide	8 6, 8, 9 5, 9	Inner-sphere monodentate and bidentate binuclear Inner-sphere monodentate (low As) or bidentate (high As)	EXAFS EXAFS	Waychunas et al. 1993 Fendorf et al. 1997
	lepidocrocite goethite	7.0	Inner-sphere bidentate-binuclear	ATR-FTIR/Raman	Goldberg and Johnston 2001
	lepidocrocite goethite	7.5, > 9.0	Inner-sphere bidentate	EXAFS	O'Reilly et al. 2001
	lepidocrocite maghemite	7.5, > 9.0	Inner-sphere bidentate	EXAFS	Randall et al. 2001
	maghemite	7.5, > 9.0	Inner-sphere bidentate	EXAFS	Manning et al. 2002
Borate	hydrated ferric oxide	7.0, 11.0	Both inner-sphere and outer-sphere Inner-sphere bidentate	RAXR EXAFS	Manning et al. 2002 Catalano et al. 2008
Citrate	goethite hydrated ferric oxide goethite	3-10 3-10 2.5-7.5	Inner-sphere Inner-sphere Inner-sphere bidentate	IR IR	Morin et al. 2008
Molybdate	ferrihydrite goethite	3-10 3-10	Inner-sphere monodentate Inner-sphere monodentate	Sorption/SCM Sorption/SCM	Su and Suarez 1995
Oxalate	goethite hematite goethite lepidocrocite	2.5-7.5 5.0 2.5-8.0 3-9	Inner-sphere bidentate Inner-sphere bidentate Both inner- and outer-sphere Inner-sphere bidentate/possibly some outer-sphere	ATR-FTIR/DRIFT ATR-IR ATR-FTIR ATR-FTIR	Cornell and Schindler 1980 Cornell and Schindler 1980 Filius et al. 1997
Phosphate	goethite lepidocrocite goethite goethite ferrihydrite hematite ferrihydrite	3-4 11.3 4-8 3-12.8 > 7.5 3.5-9.0 6.0	Inner-sphere bidentate-binuclear Inner-sphere binuclear Inner-sphere monodentate and bidentate Inner-sphere monodentate Various inner-sphere non protonated bidentate binuclear Inner-sphere bidentate-binuclear	ATR-FTIR ATR-IR ATR-FTIR DRIFT ATR-FTIR ATR-FTIR XANES	Duckworth and Martin 2001 Personn and Axe 2005 Hug and Bahmann 2006 Atkinson et al. 1974 Parfitt et al. 1975 Tejedor-Tejedor and Anderson 1990 Personn et al. 1996 Arai and Sparks 2001 Elzinga and Sparks 2007 Khare et al. 2007
Silicate	goethite ferrihydrite maghemite	3.5-11 4.0 7.0-10.8	Inner-sphere bidentate Inner-sphere bidentate Inner-sphere bidentate	Sorption/SCM ATR-FTIR ATR-FTIR	Hiemstra et al. 2007 Swedlund et al. 2009 Yang et al. 2009
Tungstate	ferrihydrite goethite	3-10 3-10	Inner-sphere monodentate Inner-sphere monodentate	Sorption/SCM Sorption/SCM	Gustafsson 2003 Xu et al. 2006

^a Extended X-ray absorption fine structure (EXAFS) spectroscopy; infrared (IR) spectroscopy; attenuated total reflectance Fourier transform IR (ATR-FTIR) spectroscopy; cylindrical internal reflection-FTIR (CIR-FTIR) spectroscopy; diffuse reflectance infrared Fourier transform (DRIFT) spectroscopy; resonant anomalous X-ray reflectivity (RAXR); surface complexation modelling (SCM).

Table S3. Fit parameters from Mössbauer analysis of solids for selected systems.

Sample	Temp (K)	CS (mm s ⁻¹)	QS (mm s ⁻¹)	H (T)	Mineral	RA (%)	Fe(II)/Fe(III)
Arsenate	77	1.26	2.83	-	Green Rust Fe(II)	71.0	2.45
		0.47	0.38	-	Green Rust Fe(III)	29.0	
	13	1.27	2.80	-	Green Rust Fe(II)	70.7	2.41
		0.48	0.38	-	Green Rust Fe(III)	29.3	
Borate	77	1.30	2.31	-	FHC	14.1	0.75
		0.39	0.00	50.6	Magnetite 1	40.2	
		0.81	-0.06	48.1	Magnetite 2	45.7	
Citrate	77	1.26	2.81	-	Green Rust Fe(II)	71.5	2.51
		0.47	0.38	-	Green Rust Fe(III)	28.5	
	13	1.27	2.78	-	Green Rust Fe(II)	71.4	2.50
		0.48	0.37	-	Green Rust Fe(III)	28.6	
Suwannee River HA	77	1.27	2.81	-	Green Rust Fe(II)	72.2	2.60
		0.47	0.37	-	Green Rust Fe(III)	27.8	
	13	1.27	2.79	-	Green Rust Fe(II)	72.2	2.60
		0.48	0.36	-	Green Rust Fe(III)	27.8	
Molybdate	77	1.26	2.82	-	Green Rust Fe(II)	70.9	2.44
		0.47	0.38	-	Green Rust Fe(III)	29.1	
	13	1.27	2.79	-	Green Rust Fe(II)	71.2	2.47
		0.48	0.36	-	Green Rust Fe(III)	28.8	
No Amendment	77	1.30	2.30	-	FHC	14.4	0.75
		0.39	-0.01	50.6	Magnetite 1	41.6	
		0.82	-0.05	48.0	Magnetite 2	44.0	
Oxalate	77	1.30	2.29	-	FHC	22.0	0.92
		0.39	-0.01	50.5	Magnetite 1	37.4	
		0.82	-0.06	47.9	Magnetite 2	40.6	
Phosphate	77	1.26	2.82	-	Green Rust Fe(II)	71.5	2.51
		0.47	0.38	-	Green Rust Fe(III)	28.5	
	13	1.27	2.80	-	Green Rust Fe(II)	71.1	2.46
		0.48	0.37	-	Green Rust Fe(III)	28.9	
Silicate	77	1.26	2.82	-	Green Rust Fe(II)	70.6	2.40
		0.47	0.38	-	Green Rust Fe(III)	29.4	
	13	1.26	2.78	-	Green Rust Fe(II)	70.0	2.33
		0.47	0.40	-	Green Rust Fe(III)	30.0	
Tungstate	77	1.26	2.82	-	Green Rust Fe(II)	70.6	2.40
		0.47	0.40	-	Green Rust Fe(III)	29.4	
	13	1.26	2.79	-	Green Rust Fe(II)	70.5	2.39
		0.47	0.40	-	Green Rust Fe(III)	29.5	

LITERATURE CITED

- Arai Y, Sparks DL. (2001). ATR-FTIR spectroscopic investigation on phosphate adsorption mechanisms at the ferrihydrite-water interface. *J. Colloid Interface Sci.* 241: 317-326.
- Atkinson RJ, Parfitt RL, Smart RSC. (1974). Infra-red study of phosphate adsorption on goethite. *J. Chem. Soc. Faraday Trans. 1* 70: 1472-1479.
- Catalano JG, Park C, Fenter P, Zhang Z. (2008). Simultaneous inner- and outer-sphere arsenate adsorption on corundum and hematite. *Geochim. Cosmochim. Acta* 72: 1986-2004.
- Chin Y-P, Aiken G, O'Loughlin E. (1994). Molecular weight, polydispersity, and spectroscopic properties of aquatic humic substances. *Environ. Sci. Technol.* 28: 1853-1858.
- Cornell RM, Schindler PW. (1980). Infrared study of the adsorption of hydroxycarboxylic acids on α -FeOOH and amorphous Fe(III) hydroxide. *Colloid Polym. Sci.* 258: 1171-1175.
- Doner LW, Douds DD. (1995). Purification of commercial gellan to monovalent cation salts results in acute modification of solution and gel-forming properties. *Carbohydr. Res.* 273: 225-233.
- Duckworth OW, Martin ST. (2001). Surface complexation and dissolution of hematite by C1-C6 dicarboxylic acids at pH = 5.0. *Geochim. Cosmochim. Acta* 65: 4289-4301.
- Elzinga EJ, Sparks DL. (2007). Phosphate adsorption onto hematite: An in situ ATR-FTIR investigation of the effects of pH and loading level on the mode of phosphate surface complexation. *J. Colloid Interface Sci.* 308: 53-70.
- Fendorf S, Eick M, Grossl P, Sparks DL. (1997). Arsenate and chromate retention mechanisms on goethite. 1. Surface structure. *Environ. Sci. Technol.* 31: 315-320.
- Filius JD, Hiemstra T, Van Riemsdijk WH. (1997). Adsorption of small weak organic acids on goethite: Modeling of Mechanisms. *J. Colloid Interface Sci.* 195: 368-380.
- Goldberg S, Johnston CT. (2001). Mechanisms of arsenic adsorption on amorphous oxides evaluated using macroscopic measurements, vibrational spectroscopy, and surface complexation modelling. *J. Colloid Interface Sci.* 234: 204-216.
- Gustafsson JP. (2003). Modelling molybdate and tungstate adsorption to ferrihydrite. *Chem. Geol.* 200: 105-115.
- Hiemstra T, Barnett MO, Van Riemsdijk WH. (2007). Interaction of silicic acid with goethite. *J. Colloid Interface Sci.* 310: 8-17.
- Hug SJ, Bahnemann D. (2006). Infrared spectra of oxalate, malonate and succinate adsorbed on the aqueous surface of rutile, anatase and lepidocrocite measured with in situ ATR-FTIR. *J. Elec. Spectros. Rel. Phenom.* 150: 208-219.
- Jansson P-E, Lindberg B, Sandford PA. (1983). Structural studies of gellan gum, an extracellular polysaccharide elaborated by *Pseudomonas elodea*. *Carbohydr. Eur.* 124: 135-139.
- Kang KS, Veeder GT, Mirrasoul PJ, Kaneko T, Cottrell IW. (1982). Agar-like polysaccharide produced by a *Pseudomonas* species: Production and basic properties. *Appl. Environ. Microbiol.* 43: 1086-1091.
- Karanfil T, Kilduff JE, Schlautman MA, Weber WJ, Jr. (1996). Adsorption of organic macromolecules by granular activated carbon. 1. Influence of molecular properties under anoxic solution conditions. *Environ. Sci. Technol.* 30: 2187-2194.
- Khare N, Martin JD, Hesterberg D. (2007). Phosphate bonding configuration on ferrihydrite based on molecular orbital calculations and XANES fingerprinting. *Geochim. Cosmochim. Acta* 71: 4405-4415.
- Manning BA, Hunt ML, Amrhein C, Yarmoff JA. (2002). Arsenic(III) and arsenic(V) reactions with zerovalent iron and corrosion products. *Environ. Sci. Technol.* 36: 5455-5461.
- Mao J, Cory RM, McKnight DM, Schmidt-Rohr K. (2007). Characterization of a nitrogen-rich fulvic acid and its precursor algae from solid state NMR. *Org. Geochem.* 38: 1277-1292.

- Morin G, Ona-Nguema G, Wang Y, Menguy N, Juillot F, Proux O, Guyot F, Calas G, Brown GE, Jr. (2008). Extended x-ray absorption fine structure analysis of arsenite and arsenate adsorption on maghemite. Environ. Sci. Technol. 42: 2361-2366.
- O'Loughlin EJ, Traina SJ, Chin Y-P. (2000). Association of organotin compounds with aquatic and terrestrial humic substances. Environ. Toxicol. Chem. 19: 2015-2021.
- O'Reilly SE, Strawn DG, Sparks DL. (2001). Residence time effects on arsenate adsorption/desorption mechanisms on goethite. Soil Sci. Soc. Am. J. 65: 67-77.
- Omoike A, Chorover J. (2006). Adsorption to goethite of extracellular polymeric substances from *Bacillus subtilis*. Geochim. Cosmochim. Acta 70: 827-838.
- Parfitt RL, Atkinson RJ, Smart RSC. (1975). The mechanisms of phosphate fixation by iron oxides. Soil Sci. Soc. Am. Proc. 39: 837-841.
- Persson P, Axe K. (2005). Adsorption of oxalate and malonate at the water-goethite interface: molecular surface speciation from IR spectroscopy. Geochim. Cosmochim. Acta 69: 541-552.
- Randall SR, Sherman DM, Ragnarsdottir KV. (2001). Sorption of As(V) on green rust ($\text{Fe}_4(\text{II})\text{Fe}_2(\text{III})(\text{OH})_{12}\text{SO}_4 \cdot 3\text{H}_2\text{O}$) and lepidocrocite ($\gamma\text{-FeOOH}$): Surface complexes from EXAFS spectroscopy. Geochim. Cosmochim. Acta 65: 1015-1023.
- Schwertmann U, Cornell RM (2000). Iron Oxides in the Laboratory. Weinheim: Wiley-VCH.
- Sørensen J. (1982). Reduction of ferric iron in anaerobic, marine sediment and interaction with reduction of nitrate and sulfate. Appl. Environ. Microbiol. 43: 319-324.
- Stookey LL. (1970). Ferrozine-A new spectrophotometric reagent for iron. Anal. Chem. 42: 779-781.
- Su C, Suarez DL. (1995). Coordination of adsorbed boron: A FTIR spectroscopic study. Environ. Sci. Technol. 29: 302-311.
- Swedlund PJ, Miskelly GM, McQuillan AJ. (2009). An attenuated total reflectance IR study of silic acid adsorbed onto a ferric oxyhydroxide surface. Geochim. Cosmochim. Acta 73: 4199-4214.
- Tejedor-Tejedor MI, Anderson MA. (1990). Protonation of phosphate on the surface of goethite as studied by CIR-FTIR and electrophoretic mobility. Langmuir 6: 602-611.
- Thorn KA, Cox LG. (2009). N-15 NMR spectra of naturally abundant nitrogen in soil and aquatic natural organic matter samples of the International Humic Substances Society. Org. Geochem. 40: 484-499.
- Waychunas GA, Rea BA, Fuller CC, Davis JA. (1993). Surface chemistry of ferrihydrite: Part 1. EXAFS studies of the geometry of coprecipitated and adsorbed arsenate. Geochim. Cosmochim. Acta 57: 2251-2269.
- Xu N, Christodoulatos C, Braida W. (2006). Modeling the competitive effect of phosphate, sulfate, silicate, and tungstate anions on the adsorption of molybdate onto goethite. Chemosphere 64: 1325-1333.
- Yang X, Roonasi P, Jolsterå R, Holmgren A. (2009). Kinetics of silicate sorption on magnetite and maghemite: An in situ ATR-FTIR study. Colloids Surfaces A: Physicochem. Eng. Aspects 343: 24-29.